The American Journal of Pathology, Vol. 169, No. 2, August 2006

DOI: 10.2353/ajpath.2006.051066

Neurobiology

Cerebral Ischemia-Hypoxia Induces Intravascular Coagulation and Autophagy

Faisal Adhami,*† Guanghong Liao,* Yury M. Morozov,‡ Aryn Schloemer,* Vincent J. Schmithorst,§ John N. Lorenz,¶ R. Scott Dunn,§ Charles V. Vorhees,* Marsha Wills-Karp,‖ Jay L. Degen,* Roger J. Davis,** Noboru Mizushima,††‡‡ Pasko Rakic,‡ Bernard J. Dardzinski,§ Scott K. Holland,§ Frank R. Sharp,§§ and Chia-Yi Kuan*

From the Department of Pediatrics, Division of Developmental Biology, the Department of Radiology,§ Imaging Research Center, and the Department of Pediatrics,‖ Division of Immunobiology, Children's Hospital Medical Center, Cincinnati, Ohio; the Physician Scientist Training Program† and the Department of Molecular and Cellular Physiology,¶ University of Cincinnati College of Medicine, Cincinnati, Ohio; the Department of Neurobiology,‡ Yale University School of Medicine, New Haven, Connecticut; the Howard Hughes Medical Institute and Program in Molecular Medicine,** University of Massachusetts Medical School, Worcester, Massachusetts; the Department of Bioregulation and Metabolism,†† The Tokyo Metropolitan Institute of Medical Science, Tokyo, Japan; Precursory Research for Embryonic Science and Technology,‡‡ Japan Science and Technology Agency, Kawaguchi, Japan; and M.I.N.D. Institute and Department of Neurology,§§ University of California at Davis, Sacramento, California*

Hypoxia is a critical factor for cell death or survival in ischemic stroke, but the pathological consequences of combined ischemia-hypoxia are not fully understood. Here we examine this issue using a modified Levine/Vannucci procedure in adult mice that consists of unilateral common carotid artery occlusion and hypoxia with tightly regulated body temperature. At the cellular level, ischemia-hypoxia produced proinflammatory cytokines and simultaneously activated both prosurvival (eg, synthesis of heat shock 70 protein, phosphorylation of ERK and AKT) and proapoptosis signaling pathways (eg, release of cytochrome *c* and AIF from mitochondria, cleavage of caspase-9 and -8). However, caspase-3 was not activated, and very few cells completed the apoptosis process. Instead, many damaged neurons showed features of autophagic/lysosomal cell death. At the tissue level, ischemia-hypoxia caused persistent cerebral perfusion deficits even after release of the carotid artery occlusion. These changes were associated with both platelet deposition and fibrin accumulation within the cerebral circulation and would be expected to contribute to infarction. Complementary studies in fibrinogen-deficient mice revealed that the absence of fibrin and/or secondary fibrin-mediated inflammatory processes significantly attenuated brain damage. Together, these results suggest that ischemia-hypoxia is a powerful stimulus for spontaneous coagulation leading to reperfusion deficits and autophagic/lysosomal cell death in brain. ***(Am J Pathol 2006, 169:566–583; DOI: 10.2353/ajpath.2006.051066)***

Hypoxia is a critical factor in cerebral ischemia. Positron emission tomography shows that the regional oxygen extraction fraction is increased in the beginning of cerebral ischemia, compensating for reduction of cerebral blood flow (CBF) to maintain the cerebral metabolic rate of oxygen close to the normal value.[1] This pattern, originally labeled "misery perfusion,"[1] is a marker of penumbra that surrounds the ischemic core.[2] Subsequently, there often occurs a reduction of oxygen extraction fraction and cerebral metabolic rate of oxygen even with the regional CBF maintained in the penumbra range, which indicates imminent infarction.[2] These results indicate decreased oxygen metabolism and suggest that hypoxia modulates the fate of ischemic tissues.

The combination of hypoxia to ischemia may trigger pathological events that are not induced by ischemia alone. One potential pathological event is hypoxia-in-

Supported by a Children's Hospital Medical Center Translational Research Initiative award and the National Institutes of Health (grant NS44315 to C.-Y.K.).

F.A. and G.L. contributed equally to this study.

Accepted for publication April 27, 2006.

R.J.D. is a Howard Hughes Medical Institute investigator.

Address reprint requests to Chia-Yi Kuan, M.D., Ph.D., Cincinnati Children's Hospital Research Foundation, Division of Developmental Biology, Room 3464, 3333 Burnet Ave., Cincinnati, OH 45229. E-mail: alex.kuan@cchmc.org.

duced fibrin deposition that results from altered anticoagulant properties of endothelial cells as demonstrated in pulmonary vessels.[3,4] Thus, the reduction of CBF in conjunction with hypoxia may induce spontaneous thrombus formation to reduce blood perfusion further. This ischemia/hypoxia-induced microvascular thrombosis may also prevent cerebral reperfusion after the release of the large artery occlusion, similar to the previously described no-reflow phenomenon after brain and cardiac ischemia.[5,6] Another potential consequence of combined ischemia-hypoxia is autophagy (self-eating), which involves the formation of autophagosomes and autophagolysosomes in degrading cellular constituents for energy production in response to nutrient deprivation.[7] Although autophagy is generally a cell survival mechanism, massive autophagy is associated with cell death.[8] The involvement of autophagy in ischemic heart and brain has only been described recently.[9–12] We postulate that the combination of ischemia and hypoxia accelerate an energy crisis and precipitate autophagy.

Among the animal models of brain ischemia, the Levine/Vannucci procedure is the only paradigm that specifically emphasizes hypoxia.[13,14] Although focal ischemia undoubtedly can induce local hypoxia, the use of systemic hypoxia in the Levine/Vannucci model produces more uniform tissue hypoxia that helps control this variable. The Levine/Vannucci model consists of unilateral common carotid artery occlusion and then subjecting animals to a hypoxic stress for a predetermined time. This model is unique in that neither the unilateral carotid occlusion nor the hypoxia alone produces brain injury, but the combination of both causes infarction.[13,14] The Levine/Vannucci procedure had been extensively used to mimic perinatal hypoxic-ischemic brain injury[14] but recently has also been applied to adult animals.[15,16] It was shown that controlling the body core temperature of adult animals at 37.5 to 37.7°C during hypoxia, typically performed by infusing hypoxic gas into a jar containing animals and submerged in a water-bath maintained at 35.5°C, produces consistent brain injury.[15] Although controlling the environmental temperature influences body temperatures of the animals inside the jar, this method may not prevent fluctuations of body temperature during the hypoxia interval. This is undesirable because it is known that small differences in brain temperature during ischemia can influence the extent of brain injury.[17] Furthermore, placing the animals inside an isolated jar precludes the ability to monitor CBF during hypoxia.

In the present study, we set out to further our understanding of the consequences of combined ischemia-hypoxia in adult brains. We have used a modified Levine/Vannucci model by controlling the core temperature of the mouse at 36.5 to 37.5°C using a heating pad on the surgical table and directly delivering hypoxic gas with anesthesia to individual animals immediately after carotid occlusion via a face mask. This modification prevents fluctuations of body temperature and allows us to monitor the changes in brain perfusion during hypoxia. We found that the combination of ischemia and hypoxia induces acute thrombosis leading to reperfusion deficits and autophagic/lysosomal processes. Taken together, these results shed new insight into the mechanism of ischemic brain injury in stroke.

Materials and Methods

Animal Surgery

The following mouse strains were used in the present study: C57BL/6 wild-type mice, GFP-LC3 transgenic mice,[18] and *fibrinogen*-null mice[19] that have been back-crossed to the C57BL/6 strain for six generations. Male mice (8 to 12 weeks of age) were used for stroke surgery. Animals were anesthetized using 0.5 to 2% isoflurane while maintaining the respiration rate at 80 to 120/minute. The right common carotid artery was occluded (RCCAO) reversibly with a releasable suture or permanently by transecting the common carotid artery between two sutures. After this, hypoxia was maintained for 30, 35, 40, or 60 minutes under anesthesia by administering 7.5% O_2 balanced with 92.5% N_2 through a gas mask. Temperature was maintained at 37 ± 0.5°C with a temperature controller (model 89000-00; Cole Parmer, Vernon Hills, IL) with a rectal probe and heating pad. After recovery from anesthesia, mice were returned to the animal care facility and inspected daily. These animal procedures were approved by the Institutional Animal Care and Use Committee and conform to the National Institutes of Health Guide for Care and Use of Laboratory Animals.

Neurological Deficit Score

Postischemia/hypoxia, animals were scored on a 6-point scale for neurological deficits based on a previous publication.[20] These are: 0, no detectable neurological deficit; 1, ptosis of eyelid ipsilateral to the occluded CCA side and/or failure to extend ipsilateral forepaw; 2, animal persistently walks in large circles toward the ipsilateral side; 3, animal persistently walks in small circles and/or rolls over repeatedly toward ipsilateral side; 4, animal lies nearly motionless on the contralateral side; 5, animal dies after recovery from the anesthesia.

Histology, Terminal dUTP Nick-End Labeling (TUNEL), and Polymerase I-Mediated Biotin-dATP Nick-Translation (PANT) Labeling

For fixation, mice were killed under deep anesthesia by transcardiac perfusion with phosphate-buffered saline containing 4% paraformaldehyde. For cryosectioning, brains were taken through graded sucrose solutions and then frozen in tissue-freezing medium. Serial coronal floating sections (100 μm for Golgi stain, 50 μm for Nissl and silver stains, 30 μm for immunohistochemistry) were cut using a vibratome or cryostat, and the eight sections corresponding to +1.98, +1.18, 0.50, 0.22, −1.06, −1.82, −2.46, and −3.28 mm to the Bregma point[21] were mounted on slides. Nissl stain was done with cresyl violet, and infarct size was measured as percent area of the

ipsilateral hemisphere using a digital image analysis system (MCID, Imaging Research Inc.; or ImageJ, National Institutes of Health). 2,3,5-Triphenylterazolim chloride (TTC) staining was done on 1-mm fresh brain sections in 2% TTC in distilled water for 30 minutes at 37°C. The silver and Golgi stains were performed with kits following the manufacturer's instruction (FD Neuro Technologies, Ellicott City, MD). Cerebral capillary permeability was tested by intraperitoneal injection of 2% Evans blue (Sigma, St. Louis, MO) at designated times after hypoxia, followed 2 hours later by fixation as above. The TUNEL labeling was performed as previously described.[22] The DNA PANT labeling was performed on paraffin-embedded sections (10 μm) using a previously described method.[23]

Cell Fractionation and Immunoblots

For mitochondrial/cytosol fractionation, brain samples (cortex or hippocampus from lesion or contralateral sides) were gently homogenized in a glass grinder in cold buffer [containing 20 mmol/L HEPES, pH 7.4, 250 mmol/L sucrose, 10 mmol/L KCl, 1.5 mmol/L $MgCl_2$, 1 mmol/L EDTA, 1 mmol/L EGTA, 0.7% protease inhibitor cocktail (Sigma), 1 mmol/L Na_3VO_4]. The mixture was centrifuged at 750 $\times$ *g* for 10 minutes to separate the pellet (P1) fraction containing the nuclei and the supernatant (S1) with mitochondria/cytosol. The nuclear fraction was resuspended in TLB (containing 20 mmol/L Tris, pH 7.4, 137 mmol/L NaCl, 25 mmol/L β-glycerophosphate, 25 mmol/L Na-pyrophosphate, 2 mmol/L EDTA, 1 mmol/L Na_3VO_4, 1% Triton X-100, 10% glycerol, 1 mmol/L phenylmethyl sulfonyl fluoride, 0.7% protease inhibitor cocktail), cooled on ice for 20 minutes, sonicated three times for 10 seconds, and then centrifuged for 20 minutes at maximum speed. The supernatant (S1) was removed and centrifuged at 8000 $\times$ *g* for 20 minutes. This pellet (P2) containing the mitochondrial fraction was resuspended in TLB, and cooled in ice and centrifuged at 140 $\times$ *g* for 10 minutes. The remaining supernatant (S2) was removed and spun in an airfuge (Beckman, Fullerton, CA) at 20 psi (100 $\times$ *g*) for 10 minutes. This supernatant (S3) contained the cytosolic fraction. For whole-cell protein purification, brain samples were homogenized as above in TLB buffer, cooled on ice for 20 minutes, sonicated, and centrifuged at 14,000 $\times$ *g* for 10 minutes. The proteins were separated by standard sodium dodecyl sulfate-polyacrylamide gel electrophoresis procedures, electrotransferred onto a polyvinylidene fluoride microporous membrane (Bio-Rad, Hercules, CA), and immunoblotted with designated antibodies followed by enhanced chemiluminescence detection (Amersham Biosciences, Arlington Heights, IL). The antibodies used in immunoblots include Hsp70 (SPA810; Stressgen, Victoria, ON, Canada), p-ERK (no. 9101; Cell Signaling, Beverly, MA), ERK1/2 (no. sc93 and sc154; Santa Cruz Biotechnology, Santa Cruz, CA), p-Akt (Ser 473, no. 9271; Cell Signaling), Akt (no. 9272; Cell Signaling), β-actin (no. A5441; Sigma), cytochrome *c* (no. 4272; Cell Signaling), AIF (no. sc9416, Santa Cruz), cytochrome oxidase subunit IV (no. A21348; Molecular Probes, Invitrogen, Carlsbad, CA), caspase-9 (no. 9504; Cell Signaling), caspase-3 (no. 9662; Cell Signaling), LC3 (generated by N. Mizushima), and LAMP-1 (no. sc5570; Santa Cruz Biotechnology).

Caspase Activity Assay

Whole-cell lysates from brain tissues were prepared as above and the concentrations were determined by Bradford assay. Equal amounts of samples were used for measuring the cleavage of Z-DEVD-AMC (for caspase-3, EnzChek caspase-3 assay kit; Molecular Probes, Invitrogen) with an excitation wavelength of 368 nm and an emission wavelength of 467 nm. The cleavage of IETD-AFC (for caspase 8) and IEHD-AFC (for caspase 9; Alexis Corp., San Diego, CA) was measured with an excitation wavelength of 400 nm and an emission wavelength of 505 nm. Every sample was analyzed three times and the average value was used, the relative fluorescence units were shown with the value in untreated samples set as 100%.

RNase Protection Assay

Quantification of the cytokine transcript levels was performed by RNase protection assay following the manufacturer's instructions. Briefly, [^{33}P]-labeled anti-sense riboprobes were synthesized using T7 MAXIscript (Ambion, Austin, TX) based on multiprobe templates (mCK2b and mCK3b from BD PharMingen, Franklin Lakes, NJ). RNA of cerebral cortex was extracted using Trizol reagent (Life Technologies, Inc., Grand Island, NY) and purified by phenol-chloroform extraction, then hybridized overnight at 56°C with the probes. The RNase digestion and precipitation of protected fragments were completed using the RPA III kit (Ambion). After separation via electrophoresis with a 5% acrylamide, 8 mol/L urea, and 1$\times$ TBE gel, the radioactivity was measured by exposure to a phosphorimager screen (Molecular Devices, Sunnyvale, CA) and quantified.

Enzyme-Linked Immunosorbent Assay (ELISA)

Measurements of protein levels for interleukin (IL)-1β and IL-6 in the mouse brain were performed using ELISA and following the manufacturer's instructions (R&D Systems, Minneapolis, MN). Briefly, 96-well plates were coated with the capture antibody overnight and then blocked (1% bovine serum albumin, 5% sucrose, 0.05% NaN_3). Standards of IL-1β and IL-6 (5000 to 0 pg/ml in triplicates) or samples [homogenates from each mouse hemisphere in 500 μl of phosphate-buffered saline (PBS), using 50 μl per well in duplicates] were then added to the plates for 2 hours. Protein concentrations were determined using a streptavidin-peroxidase substrate system and biotinylated detection antibodies, and the plates were read at 450 nm with 595 nm background subtraction.

Electron Microscopy

Animals were exposed to ischemia-hypoxia, and after 6 hours of recovery, anesthetized, and perfused transcardially with 4% paraformaldehyde and 1% glutaraldehyde in 0.1 mol/L phosphate buffer. The brains were removed and coronal 100-μm-thick sections were cut by a vibratome. The sections were postfixed with 1% OsO_4, dehydrated, and embedded in Durcupan (ACM; Fluka, Buchs, Switzerland) on a microscope slide and coverslipped. Fragments of cerebral cortex from damaged and contralateral hemispheres were re-embedded into Durcupan blocks and cut by a Reichert ultramicrotome into 70-nm-thick sections. The ultrathin sections were then stained with uranil acetate and lead citrate and evaluated in a JEOL 1010 electron microscope.

GFP-LC3 Immunofluorescence

Mice expressing the GFP-LC3 fusion protein have been characterized.[18] These mice have been used to monitor autophagy in cells because the GFP-LC3 protein normally has a diffuse, cytoplasmic distribution but is shifted to bright, punctate dots on autophagy. These mice were subjected to ischemia-hypoxia as described above for 40 minutes and analyzed for immunohistochemistry as described above after either 6 or 18 hours of recovery. Sections were stained with a rabbit monoclonal antibody against GFP (no. A11122; Molecular Probes, Invitrogen) and ethidium homodimer (2 μmol/L, no. E1169; Molecular Probes) and sections were analyzed using a Zeiss (Zeiss, Jena, Germany) confocal microscope (LSM-510). Each time point was analyzed in four different animals.

Laser Doppler Flowmetry

The CBF was measured using a Periflux 5010 laser Doppler perfusion system (Perimed, Jarfalla, Sweden) with a model 407 probe mounted directly on the skull over the right forebrain. Data were recorded during a 2-minute baseline period, for 2 minutes after the suture was tightened, throughout 40 minutes of hypoxia, and for 20 minutes after restoration to normoxia. Mice that died during hypoxia were excluded from average due to an exaggerated drop in perfusion. Data are presented as a percentage of baseline and were averaged as follows: three mice each for hypoxia, reversible ischemia, or permanent ischemia alone; seven mice for permanent ischemia with hypoxia; five for reversible ischemia with hypoxia. For studies in fibrinogen-deficient and heterozygous mice, three mice for each genotype were analyzed and averaged, focusing on three data points: blood flow averaged throughout 1 minute of right common carotid occlusion alone, throughout 10 minutes during hypoxia (25 to 35 minutes), and throughout 10 minutes during recovery (10 to 20 minutes recovery).

Carotid Blood Pressure and Blood Flow

Mice were anesthetized as described with isoflurane. The right common carotid was isolated and occluded using a single suture. Then, on the side of the suture proximal to the heart, the right common carotid artery was cannulated with polyethylene tubing. The catheter was connected to a COBE CDXIII fixed-dome pressure transducer (COBE Cardiovascular, Arvada, CO) for measurement of arterial blood pressure. To determine carotid blood flow to the brain after RCCAO, the left common carotid artery was isolated and a Transonics Systems (Ithaca, NY) 0.5SB series perivascular flow probe placed over the artery. Flow signals from a Transonic System model TS420 transit time flowmeter and pressure signals from the mentioned pressure transducer were recorded at a sampling rate of 1000 samples per second per channel and analyzed using a MacLab 4/s (ADInstruments, Colorado Springs, CO) data acquisition system. Heart rate and cerebrovascular resistance was calculated using the software from recordings. Data obtained were averaged from three mice.

Arterial Blood Gases

Cerebral hemispheric ischemia/hypoxia was performed as described above. Blood was collected by the tail clip method. Mice were heated to 39°C just before the collection times to induce flushing of the tail with predominantly arterial blood. Approximately 150 μl of blood was collected in heparinized capillary tubes before hypoxia, 2 minutes before the end of hypoxia, and 30 minutes into recovery and analyzed with an i-Stat portable clinical analyzer with a CG8+ cartridge (Abbott Laboratories, Abbott Park, IL). Data obtained were averaged from five mice.

Magnetic Resonance Imaging

All images were acquired on a Bruker 7T/30 cm imaging spectrometer with a 20 G/cm gradient coil insert. Radiofrequency (RF) excitation was with a 72-mm-volume coil and RF reception was with a surface coil. Details for the three imaging sequences are described below.

T2-Weighted Images

Spin-echo RARE sequence, TR/TE = 5000/83 ms, rare factor = 6, imaging BW = 75 kHz, FOV = 25.6 $\times$ 25.6 mm, matrix = 256 $\times$ 192, slice thickness = 0.75 mm, NEX = 2.

Arterial Spin Labeling Perfusion

FLASH sequence, TR/TE = 25/3.5 ms, imaging BW = 50 kHz, FOV = 25.6 $\times$ 25.6 mm, matrix = 128 $\times$ 128, slice thickness = 2.0 mm, tagging slab thickness = 7 mm. Forty-eight total images were acquired, with 24 tagged images alternated with 24 control images. In

the tagged images, the tagging slab was placed inferior to the imaging plane to saturate the incoming blood; in the control images, the tagging was placed superior to the imaging plane (to make any magnetization transfer effects identical for tagged and control images). Percent change maps were calculated from the difference in signal intensities between the tagged and control images.

Diffusion

Four-segment diffusion-weighted spin-echo EPI sequence, TR/TE = 2500/26 ms, imaging BW = 250 kHz, FOV = 25.6 × 25.6 mm, matrix = 128 × 128, slice thickness = 1.0 mm. Three images were acquired with no diffusion weighting. Twelve diffusion-weighed images were acquired with $\delta = 5$ ms, $D = 13$ ms, b value = 1000 seconds/mm^2, and diffusion gradient directions of (1.0, 0.5, 1.0), (1.0, −0.5, 1.0), (0.5, 1.0, 1.0], (−0.5, 1.0, 1.0), (1.0, 1.0, 0.5), (1.0, 1.0, −0.5) (two images acquired for each direction). Components of the diffusion tensor were calculated from a least-squares fit of the logarithm of the signal intensities and the directionally averaged apparent diffusion coefficient (ADC) was obtained by averaging the diagonal elements.

Histological Assay of Brain Perfusion and Coagulation

Perfusion status was measured using a modification of a published procedure.[24] Briefly, fluorescein isothiocyanate (FITC)-dextran (5 mg in 100 μl PBS of 2 × 10^6 MW; Sigma) was injected with a small-bore needle into the left ventricle of mice 1 or 3 hours after ischemia/hypoxia. After 2 minutes, the animal was rapidly decapitated and the brain was removed and postfixed for 48 hours. Sections were cut as above and analyzed with fluorescence microscopy. For quantification in fibrinogen studies, images obtained were analyzed using ImageJ software. An index of perfusion was measured in an area excluding the midline (matching the maximal possible infarction) as the number of FITC pixels per number of total pixels in maximal infarct area of ipsilateral hemisphere. This was then normalized to the equivalent measurement on the contralateral side to account for potential animal global perfusion variation. Immunohistochemistry was performed using a rat monoclonal antibody against P-selectin (no. 550289; BD PharMingen, San Diego, CA), a rabbit polyclonal antibody against fibrin/fibrinogen,[19] and a rat monoclonal antibody against glycoprotein IIb (CD41, no. 553847; BD PharMingen).

Statistical Analysis

Quantitative data were compared between experimental and control groups using Microsoft Excel's two-sample (unpaired) t-test assuming equal variance.

Results

Determining the Effect of Hypoxia Duration on Brain Damage Consistency

Male C57BL/6 mice (8 to 12 weeks old) were subjected to combined cerebral ischemia-hypoxia. Mice were anesthetized with isoflurane delivered with pure oxygen through a face mask, and the right common carotid artery (RCCA) was ligated while the core temperature of the animal was maintained at 36.5 to 37.5°C using a rectal thermometer and a heating pad. Immediately after occlusion of the RCCA and closure of the surgical wound, the gas was switched to 7.5% oxygen and 92.5% nitrogen to initiate hypoxia for a predetermined period. During hypoxia, mice were allowed to breathe spontaneously with the respiration rate maintained at 100 to 120 breaths per minute by adjusting the concentration of isoflurane, typically between 0.5 to 1.0%. At the end of the hypoxic period, the mice were removed from the anesthesia machine and returned to the animal care facility. At various times after ischemia-hypoxia challenge, mice were examined and scored for neurological deficits (NDS) on a 6-point scale[20] (Figure 1A). The extent of brain infarction was quantified using Nissl staining (Figure 1, B–F). Our initial goal was to determine the minimal duration of hypoxia that produces consistent brain damage, and then use it to characterize the progression of brain damage at different times after ischemia-hypoxia.

In 10 C57BL/6 mice subjected to RCCA occlusion and 30-minute hypoxia, 50% of the mice showed a NDS of 3 (persistently walking in a small circle toward the CCA-occluded side; see example in Figure 1A), 4 (lying motionlessly on the contralateral side), or 5 (fatal) at 48 hours. Lengthening the duration of hypoxia to 35 or 40 minutes caused an NDS greater than 3 in more than 70% of the mice at 24 hours (Figure 1A). The highest mortality rate (33% for the 40-minute hypoxia group) is similar to that reported in a previous study using the jar and water bath (42% for 30-minute hypoxia in Vannucci et al[15]). In separate trials, increasing the recovery time to 6 days after ischemia-hypoxia led to higher mortality.

We then examined the extent of brain injury in all surviving animals at the indicated recovery time after different durations of hypoxia (Figure 1A). The brains were serial sectioned (50-μm-thick sections) and eight representative sections spanning from +2.0 to −3.2 mm to Bregma were stained with cresyl violet and the areas of infarction quantified (Figure 1, B–F). This analysis showed that lengthening the hypoxia duration to 40 minutes increases the average infarcted area to ~60% of the hemisphere and reduces individual variability (Figure 1, compare B, C, and E). Increasing the recovery time to 6 days after 30- and 35-minute hypoxia reduces the average infarcted area, presumably because the mice with larger infarcts have already died (Figure 1, compare C and D and E and F). We initially attempted to use a ventilator to control the amount of delivered hypoxic gas to increase the consistency of brain damage, but quickly

A

Hypoxia duration	30 min		35 min		40min
Survival period	48hr (n=10)	6d (n=10)	24hr (n=10)	6d (n=10)	24hr (n=9)
NDS 1–2	50%	50%	30%	60%	23%
NDS 3–4	30%	0%	50%	0%	44%
NDS 5	20%	50%	20%	40%	33%

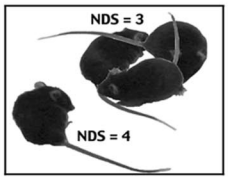

Figure 1. Carotid occlusion and 40-minute hypoxia produces consistent infarction. **A:** Outcomes of mortality (NDS = 5) and neurological deficits after different durations of hypoxia and survival times. The montage picture shows a mouse with a neurological deficit score (NDS) of 3 (small circling) and another with a NDS of 4 (immobilization). **B–F:** Quantification of the infarct area by Nissl staining on the surviving animals in conditions indicated in **A**. A hypoxic duration of 30 (**E**, **F**) and 35 minutes (**C**, **D**) produces smaller average infarct size and more variable brain damage in individual animals than 40-minute hypoxia (**B**). Eight rostral-to-caudal brain levels spanning from 2.0 to −3.2 mm to the Bregma point were analyzed. Open squares indicate results in individual animals; closed circles and bars indicate the average infarct size and the SE of each group, respectively.

abandoned this procedure because most animals died during hypoxia because of a rapid blood pressure decline. This is probably because the positive pressure delivered by the ventilator reduced the venous return to the chest cavity, suppressed the cardiac output, and made the animal unable to compensate for hypoxia-induced hypotension (Figure 3C). Thus, for the remainder of this study, unless specified otherwise, we applied 40-minute hypoxia (7.5% oxygen) after permanent RCCA ligation to 8- to 12-week-old male C57BL/6 mice to examine the pathological consequences of cerebral ischemia-hypoxia.

Progression of Brain Edema and Infarction after Ischemia-Hypoxia

To characterize the progression of brain pathology, we analyzed animals at 6 or 24 hours after ischemia-hypoxia to examine the permeability of the blood-brain-barrier (BBB) by intravenous injection of the Evans blue dye (Figure 2, A, B, D, and E) and tissue infarction by TTC staining (Figure 2, C, G, and H). At 6 hours after ischemia-hypoxia, there was no appreciable extravasation of Evans blue dye to the brain (Figure 2A), but the size of the lateral ventricle on the right side was consistently smaller in serial sections (Figure 2B, $n > 4$). This pattern indicates cytotoxic edema associated with preserved BBB integrity.[25] In contrast, there was gross extravasation of the Evans blue dye and hemorrhage in the brain at 24 hours, indicating BBB breakdown and the onset of vasogenic edema (Figure 2, D and E; $n > 4$). Magnetic resonance imaging (MRI) also showed a large area of increased T2-relaxation time on the carotid artery-occluded side at 24 hours, indicating brain edema (Figure 2F, $n > 6$). The effects of the severe brain edema are manifested by compression of the ventricles and a shift of the midline (Figure 2F), which may lead to fatal cerebral herniation. Thus, cerebral ischemia-hypoxia first induces cytotoxic edema, and then increases BBB permeability leading to vasogenic edema.

Examination of a group of eight mice by TTC staining showed that the brain infarction was restricted to the striatum and anterior cerebral cortex at 6 hours, corresponding to the middle cerebral artery (MCA) territory (Figure 2C). Noticeably, none of these mice showed damage in the hippocampus at this time. When the extent

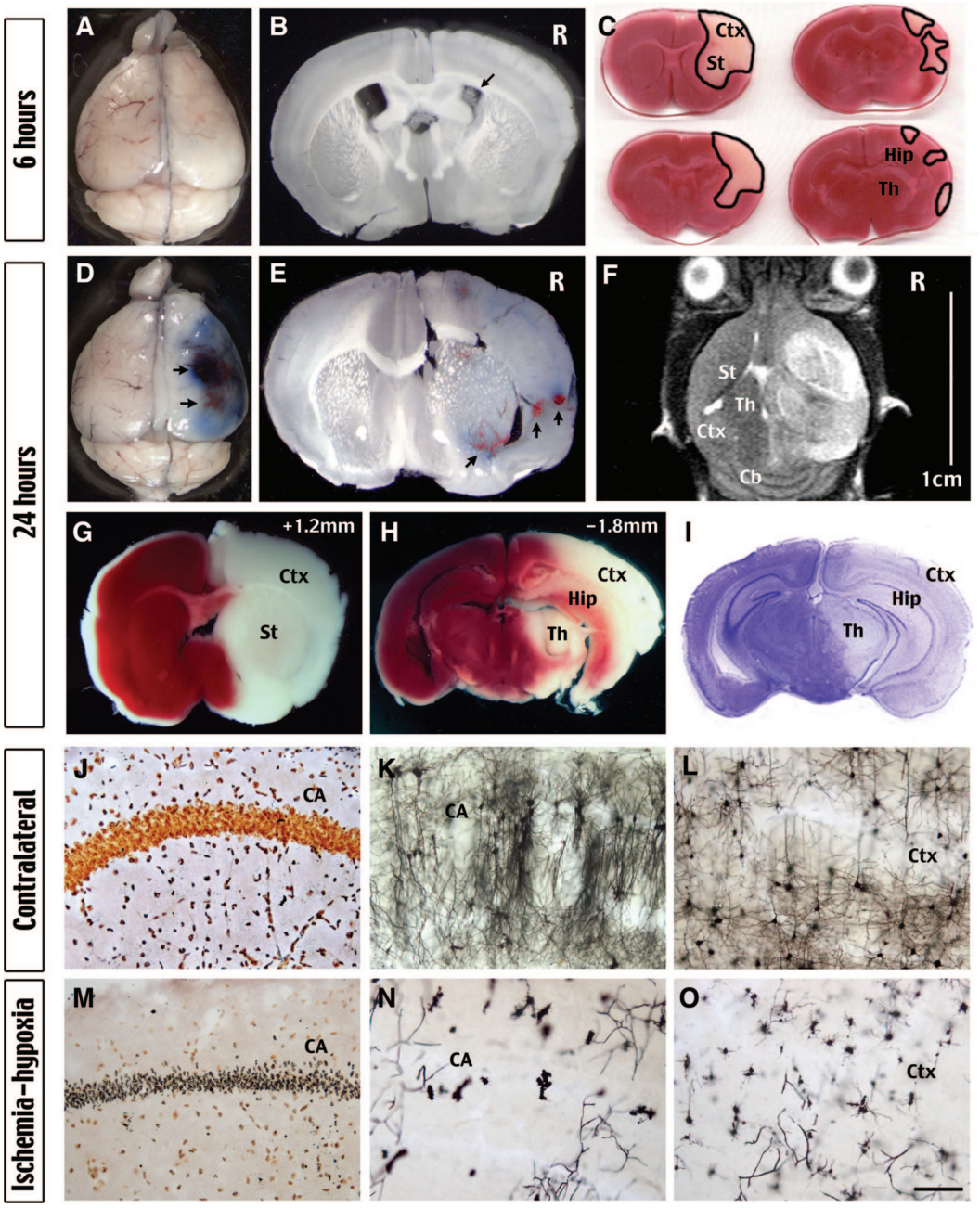

Figure 2. Ischemia-hypoxia causes progression of brain infarction originating from the MCA territory and breakdown of the BBB. **A** and **B:** There is no extravasation of the Evans blue dye at 6 hours after ischemia-hypoxia, but the lateral ventricule on the presumptive lesion side consistently is reduced (**arrow** in **B**), indicating brain edema. **C:** TTC stain of brain slices shows the worst pathology of a group of eight mice at 6 hours after ischemia-hypoxia. Note the brain infarction was limited to the MCA territory including the striatum (St) and the rostral cerebral cortex (Ctx). **D** and **E:** Vast extravasation of the Evans blue dye and hemorrhagic transformation (**arrows**) by 24 hours after ischemia-hypoxia indicate the breakdown of the BBB. **F:** A representative T2-weighted MR image shows increased brain edema in a large portion of the hemisphere covering the cerebral cortex (Ctx), the striatum (St), and the thalamus (Th), but sparing the cerebellum (Cb). The severe brain edema causes a midline-shift and compression of the ventricles. **G–I:** Brain infarction exhibits as lack of TTC stain (**G**, **H**) and reduced Nissl's stain (**I**) in structures as in **F** in addition to the hippocampus (Hip). **J** and **M:** Silver stain shows degeneration of the hippocampal pyramidal neurons on the lesion side (**M**), but not the contralateral side (**J**) at 24 hours after ischemia-hypoxia. **K**, **L**, **N**, and **O:** Golgi stain shows extensive degeneration of hippocampal pyramidal neurons (CA in **N**) and cortical neurons (Ctx in **O**). The hippocampus (**K**) and the cortex (**L**) on the contralateral side retain abundant axons and dendrites showing no signs of injury. Shown are the representative pictures of at least four mice for each staining. Scale bars: 1.5 mm (**K**, **L**, **N**, **O**); 300 μm (**J**, **M**).

of brain injury at 24 hours was assessed by the TTC and Nissl stains, it showed a large area of infarction including striatum, cerebral cortex, hippocampus, thalamus, and amygdala (Figure 2, G–I). Silver and Golgi stains of brains at 24 hours also showed extensive neuronal loss in the hippocampus (Figure 2, J, K, M, and N) and the striatum (data not shown). Although the loss of neurons was less in the cerebral cortex, there was prominent and extensive destruction of the neurites in this area (Figure 2, L and O). Together, these results suggest that unilateral carotid occlusion and hypoxia induces infarction that originates in the MCA territory and spreads to the anterior

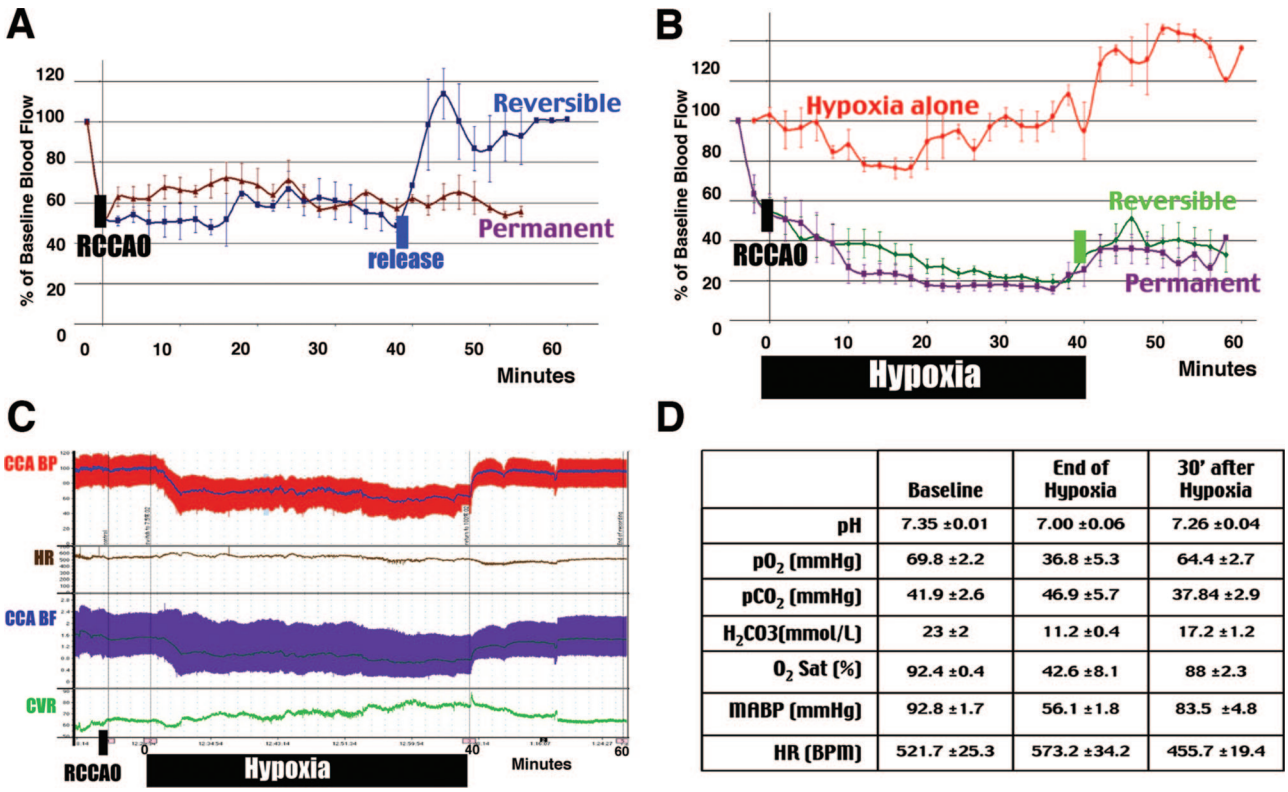

	Baseline	End of Hypoxia	30' after Hypoxia
pH	7.35 ±0.01	7.00 ±0.06	7.26 ±0.04
pO_2 (mmHg)	69.8 ±2.2	36.8 ±5.3	64.4 ±2.7
pCO_2 (mmHg)	41.9 ±2.6	46.9 ±5.7	37.84 ±2.9
H_2CO3(mmol/L)	23 ±2	11.2 ±0.4	17.2 ±1.2
O_2 Sat (%)	92.4 ±0.4	42.6 ±8.1	88 ±2.3
MABP (mmHg)	92.8 ±1.7	56.1 ±1.8	83.5 ±4.8
HR (BPM)	521.7 ±25.3	573.2 ±34.2	455.7 ±19.4

Figure 3. Combined ischemia-hypoxia diminishes CBF and impedes reperfusion. **A:** Laser Doppler flowmetry shows 50% reduction of the baseline CBF and a fast reperfusion after release of the right common carotid artery occlusion (RCCAO). **B:** Hypoxia alone has little effect on the CBF. In contrast, the combination of RCCAO and hypoxia diminished the CBF to ~20% of the normal value, which recovered poorly even with a reversible carotid occlusion ($n > 3$ for each condition). **C:** While the carotid artery pressure (BP) and flow (BF) are maintained at ~60% of the baseline level, the cerebrovascular resistance (CVR) steadily increases during hypoxia. **D:** Measurement of the blood gas parameters ($n = 5$) and the mean arterial BP and HR ($n = 3$) indicates a transient change of all values that primarily recover at 30 minutes after hypoxia.

cerebral artery and portions of the posterior cerebral artery territories. The major unaffected areas include the midline regions, which likely have better collateral blood flow, and the cerebellum, which is mainly supplied by the vertebral arteries.

Imposing Hypoxia to Ischemic Brain Further Reduces Blood Flow and Impedes Reperfusion

Previous studies indicated that a high probability of infarction (>95%) in brain tissue occurs when the regional cerebral blood flow (rCBF) declines to <25% of control for a prolonged time, whereas 50% reduction of the CBF only causes a low probability of infarction (<5%).[26] It is unlikely that unilateral carotid occlusion alone can reduce the CBF to <25% due to compensation by the circle of Willis, but how superimposing hypoxia to unilateral carotid occlusion affects the CBF is unclear. Hence, we used laser Doppler flowmetry to examine the changes of CBF in the MCA territory after unilateral common carotid artery occlusion (RCCAO) and hypoxia (Figure 3).

We found that RCCAO by itself diminished the rCBF to ~50% of the preocclusion value for up to 60 minutes, which quickly returned to normal after release of the carotid occlusion (Figure 3A). Subjecting the mouse to 7.5% oxygen alone triggered an initial reduction of CBF, but it quickly returned to normal values presumably because of autoregulation of the cerebral circulation under hypoxic conditions (Figure 3B).[27] However, the combination of RCCA ligation and hypoxia caused a gradual decline of CBF to 20% of the preocclusion value, and it only returned to 30 to 40% after an interval of 40-minute hypoxia. Moreover, release of the RCCA occlusion did little to improve the CBF level after hypoxia (Figure 3B). These results show that superimposing hypoxia on unilateral carotid occlusion-induced partial ischemia can severely reduce the rCBF to a degree similar to that in focal ischemia models, and it has persistent negative effects on cerebral reperfusion. This effect is similar to the previously described no-reflow phenomenon after brain ischemia.[5]

Simultaneous measurement of the right carotid blood pressure (BP) and the left carotid blood flow (BF) showed that both were suppressed, yet maintained at a stable level throughout the hypoxia period (Figure 3C). In contrast, the cerebral vascular resistance, measured by dBP/dBF, steadily increased during the hypoxia interval (Figure 3C). The arterial blood gases showed that pH declined (from 7.35 to 7.00), oxygen tension decreased (pO_2, from 69.8 to 36.8 mmHg), as did oxygen saturation (O_2 Sat, from 92.4 to 56.1%) during ischemia-hypoxia. However, these parameters all returned to near normal values by 30 minutes after hypoxia (pH from 7.00 to 7.26; pO_2 from 36.8 to 64.4 mmHg; O_2 Sat from 42.6 to 88%,

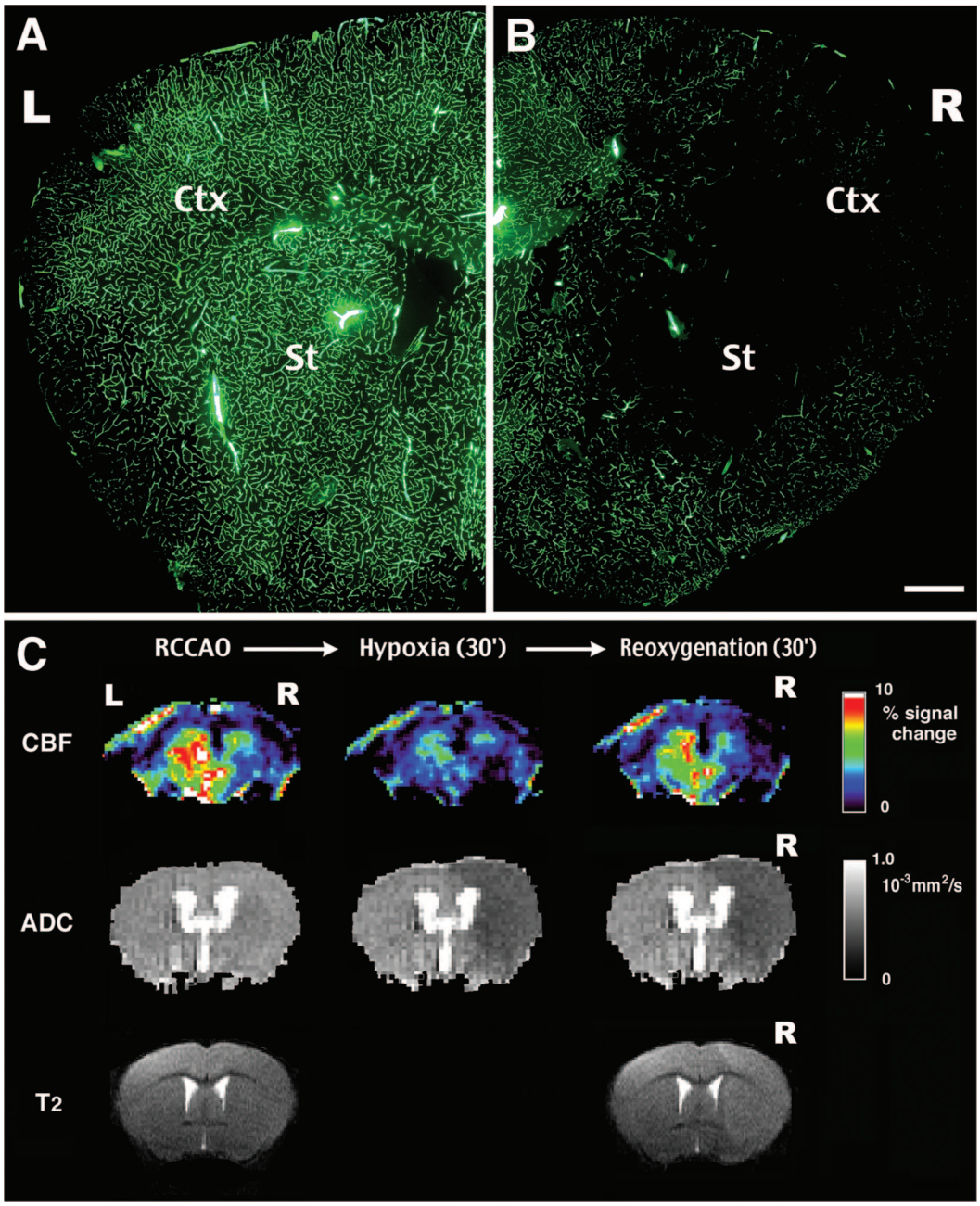

Figure 4. Perfusion deficits after ischemia-hypoxia are prolonged well into recovery. **A** and **B:** Intracardiac injection of FITC-dextran at 3 hours after ischemia-hypoxia fills vessels of the contralateral side of the brain (**B**), but is excluded in a large area including the striatum (St) and the cortex (Ctx) on the lesion side (**C**). FITC-dextran images are representative for six animals. **C:** Sequential magnetic resonance images (MRIs) of a mouse brain after RCCAO (**left**), at 30 minutes of hypoxia (**center**), and at 30 minutes of recovery of hypoxia (**right**). **Top row** is the relative CBF map measured by the arterial spin labeling method. **Middle row** is the corresponding ADC map. **Bottom row** is the T2-weighted image at the beginning and the end of MRI tracing. MRI tracing shows ADC reduction and prolonged T2-relaxation in the hemisphere ipsilateral to RCCAO. Details of the MR imaging sequences are provided in the Materials and Methods section. Scale bar = 1 mm.

Figure 3D). Thus, the hypoxia-induced reperfusion deficits and brain infarction cannot be attributed to protracted systemic hypotension or oxygen deprivation.

To test whether combined ischemia-hypoxia produces persistent reperfusion defects, we used fluorescein-conjugated dextran as a tracer to examine the patency of brain vessels at 1 or 3 hours after the unilateral carotid occlusion and 40-minute hypoxia. This analysis showed a large area of vascular obstruction in the striatum and the anterior cerebral cortex on the carotid-ligated side of the brain (Figure 4B). This area of vascular obstruction is almost identical to the area that infarcts first in this model (Figure 2C). In contrast, there was no obvious vascular obstruction on the contralateral side of the brain (Figure 4A) or after unilateral carotid occlusion alone (data not shown).

The persistent perfusion impairment correlated with increased cerebrovascular resistance could have several

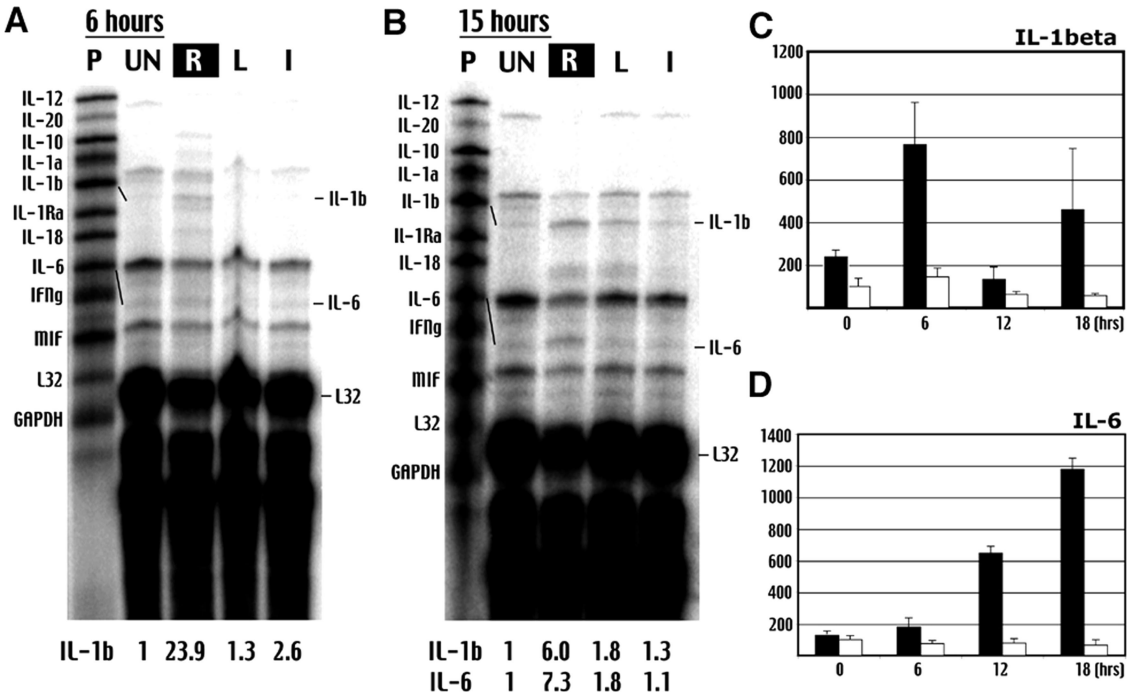

Figure 5. Cerebral ischemia-hypoxia causes a bi-phasic pattern of cytokine induction. **A** and **B:** Ribonuclease protection assay shows early induction of IL-1β and delayed production of IL-6 transcripts after ischemia hypoxia. P, Free probe; UN, samples from unchallenged brains; R, ischemia-hypoxia-challenged/right side of the brain; L, contralateral/left side of brain, I, unilateral CCA occlusion/ischemia alone. The increase of transcript is quantified against the housekeeping gene *L32*. Shown is the representative data in three sets of experiments. **C:** The ELISA shows a bi-phasic increase of IL-1β on the ipsilateral side (**filled columns**), but not on the contralateral side of the brain (open columns) after ischemia-hypoxia. **D:** In contrast, IL-6 level increases gradually after ischemia-hypoxia. Shown are the average quantities with the SE in whole-brain samples at the indicated times after ischemia-hypoxia (hours) ($n > 4$ for each point).

causes. Vasoconstriction is less likely because hypoxia typically triggers vasodilation.[27] To analyze the involvement of edema-related vessel compression, we used MRI to monitor the changes of cerebral perfusion (CBF), water diffusion (ADC), and water accumulation (T2 relaxation time) in the same animal after unilateral carotid occlusion and hypoxia (Figure 4C). To do so, the CBF was measured by the arterial spin labeling[28] technique to avoid the use of paramagnetic dyes. This longitudinal study revealed that unilateral carotid occlusion did not reduce ADC, but a large area of decreased ADC emerged at 25 minutes after the combined ischemia-hypoxia. Moreover, the ADC on the ipsilateral side continued to decrease at 30 minutes after hypoxia and was accompanied by an increase of the T2 relaxation time (Figure 4C, bottom right). The reduction of ADC indicates the accumulation of water in the diffusion-restricted intracellular space or the extracellular pathway with increased tortuosity.[29] This result suggests that ischemia-hypoxia induces acute brain edema that may impair the CBF after the hypoxia interval. Another possible cause of persistent impairment of the CBF is thrombus formation. Additional experiments demonstrate that combined cerebral ischemia-hypoxia does indeed trigger intravascular thrombosis (see Figures 9 and10).

Ischemia-Hypoxia Triggers Cytokine Production and Incomplete Apoptotic Signaling

The broad regions of infarction and massive brain edema produced by the modified Levine/Vannucci model resemble clinical situations of large hemispheric stroke.[30] Because the extent of brain damage surpasses those incurred by the commonly used transient middle cerebral artery occlusion (MCAO) model, we investigated whether these two models trigger similar or different mechanisms of cell death. To address this issue, we examined three classes of signal transduction pathways that have been implicated in the MCAO model. These are IL-1β and other proinflammatory cytokines;[31,32] cytoprotective HSP70, ERK, and AKT pathways;[33–35] and proapoptotic pathways including the mitochondrial release of cytochrome *c* and apoptosis-inducing factor (AIF) and activation of caspases.[36–39]

Ribonuclease protection assay showed that IL-1β mRNA was increased 23.9-fold at 6 hours and 6.0-fold at 15 hours after ischemia-hypoxia in the carotid-occluded side of brain (Figure 5, A and B). In contrast, IL-6 mRNA was not detected until 15 hours. ELISA analysis showed a biphasic pattern of IL-1β protein induction: it increased 2.25-fold by the end of hypoxia, 7.65-fold at 6 hours, declined to 1.30-fold at 12 hours, and increased again to 4.6-fold at 18 hours (Figure 5C). A similar pattern of biphasic IL-1β induction was reported in the MCAO model of stroke.[40] Consistent with the ribonuclease protection assay data, ELISA analysis showed that the protein level of IL-6 rises steadily after ischemia-hypoxia: it increases to 1.8-fold at 6 hours, 6.5-fold at 12 hours, and 11.75-fold at 18 hours (Figure 5D).

To examine the signaling pathways preceding infarction, we extracted proteins from the hippocampus of both sides of the brain at 1, 6, and 24 hours after ischemia-

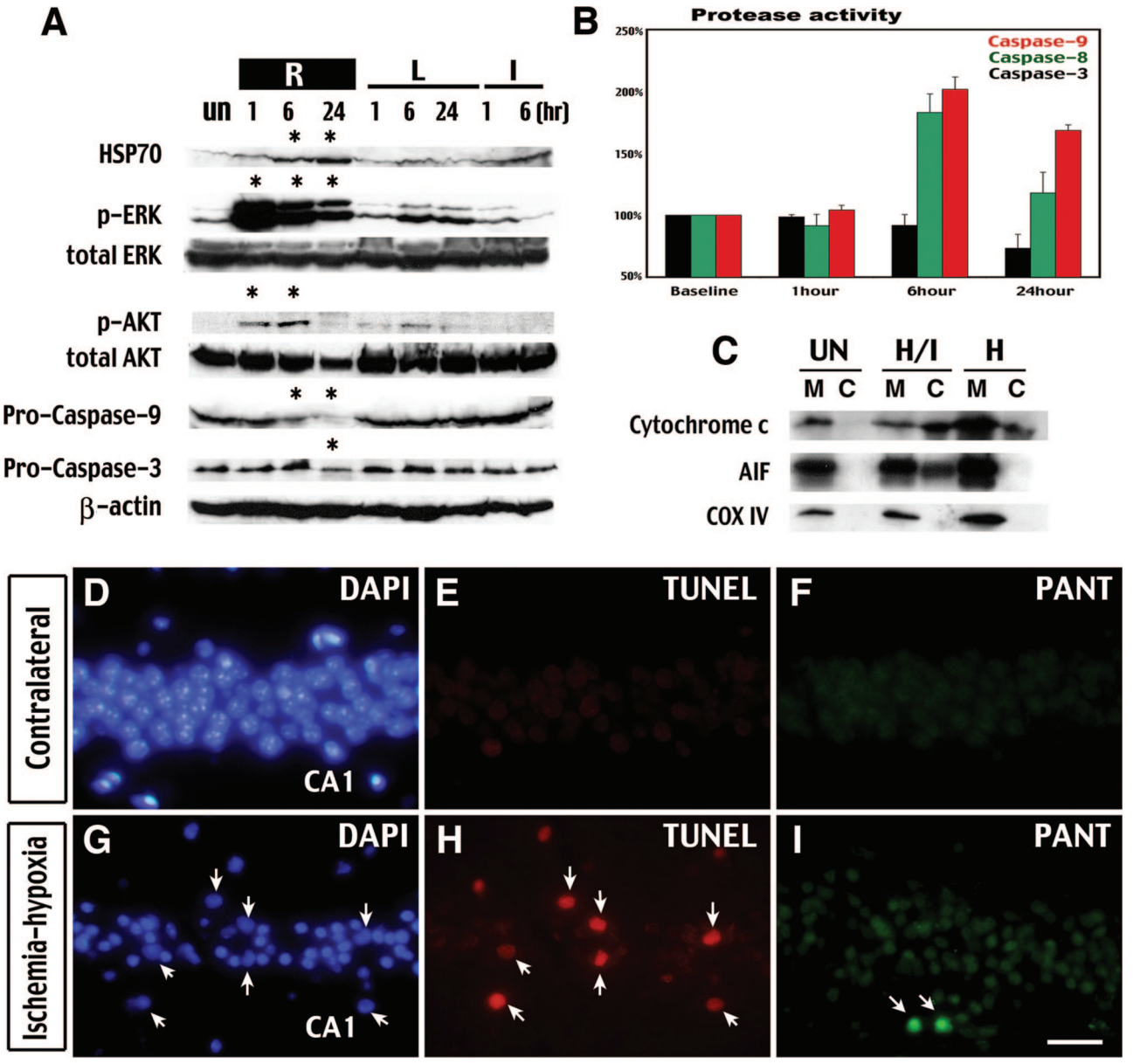

Figure 6. Cerebral ischemia-hypoxia causes prosurvival signaling and aborted apoptosis in initially viable tissues. **A:** Immunoblot shows more pronounced accumulation of Hsp70 and phosphorylation of ERK and AKT in the hippocampus on the lesion side (R) than the contralateral side (L) at indicated times after ischemia-hypoxia or unilateral CCA occlusion (I). This is accompanied by a degradation of pro-caspase 3 and 9 on the lesion side (R). **B:** Protease activity assay shows increased caspase-9 and -8 activities, but not caspase-3 activity, at 6 and 24 hours after ischemia-hypoxia. **C:** Cell fractionation and Western blot analysis indicates the release of cytochrome *c* and AIF from the mitochondria (M) to the cytosol (C) in the hippocampus at 6 hours after ischemia-hypoxia. The purity of the mitochondria/cytosol fractioning is shown by immunoblotting against the cytochrome oxidase (COX) subunit IV. **D–I:** PANT stain shows single-strand DNA breaks in the CA1 region of the hippocampus at 24 hours after ischemia-hypoxia (**I**), with some TUNEL-positive cells detected in adjacent sections (**H**). Even fewer TUNEL-positive cells were detected in other regions of the brain. Biochemical data are representative of three sets of experiments with the sample pooled from at least three animals of each time point. PANT and TUNEL staining are representative for three animals analyzed at both 6 and 24 hours. Scale bar = 400 μm.

hypoxia to compare with the samples collected after unilateral carotid occlusion alone (Figure 6A). We found that ERK and AKT phosphorylation increased at 1 and 6 hours after ischemia-hypoxia, when this region is still viable (Figure 2C), and decreased at 24 hours when this region is severely damaged (Figure 2, H, I, M, and N). In contrast, the protein level of Hsp70 continually increased up to 24 hours (Figure 6A). An identical pattern of Hsp70, ERK, and AKT induction was also detected in the cerebral cortex (data not shown). These results suggest that carotid occlusion plus 40-minute hypoxia induces prosurvival signaling in the stressed, but viable, brain regions before they convert to infarction.

Cytochrome *c* and AIF were released from the mitochondria (M) into the cell cytoplasm (C) in the hippocampus and the cerebral cortex at 6 hours after ischemia-hypoxia (H/I in Figure 6C). On immunoblot, a decrease of pro-caspase-9 and caspase-3 protein levels started at 6 and 24 hours after ischemia-hypoxia, respectively (Figure 6A). The protease activities of caspase-9 and -8 were also increased at 6 and 24 hours (Figure 6B). However, there was no increase of caspase-3 activity (Figure 6B) or

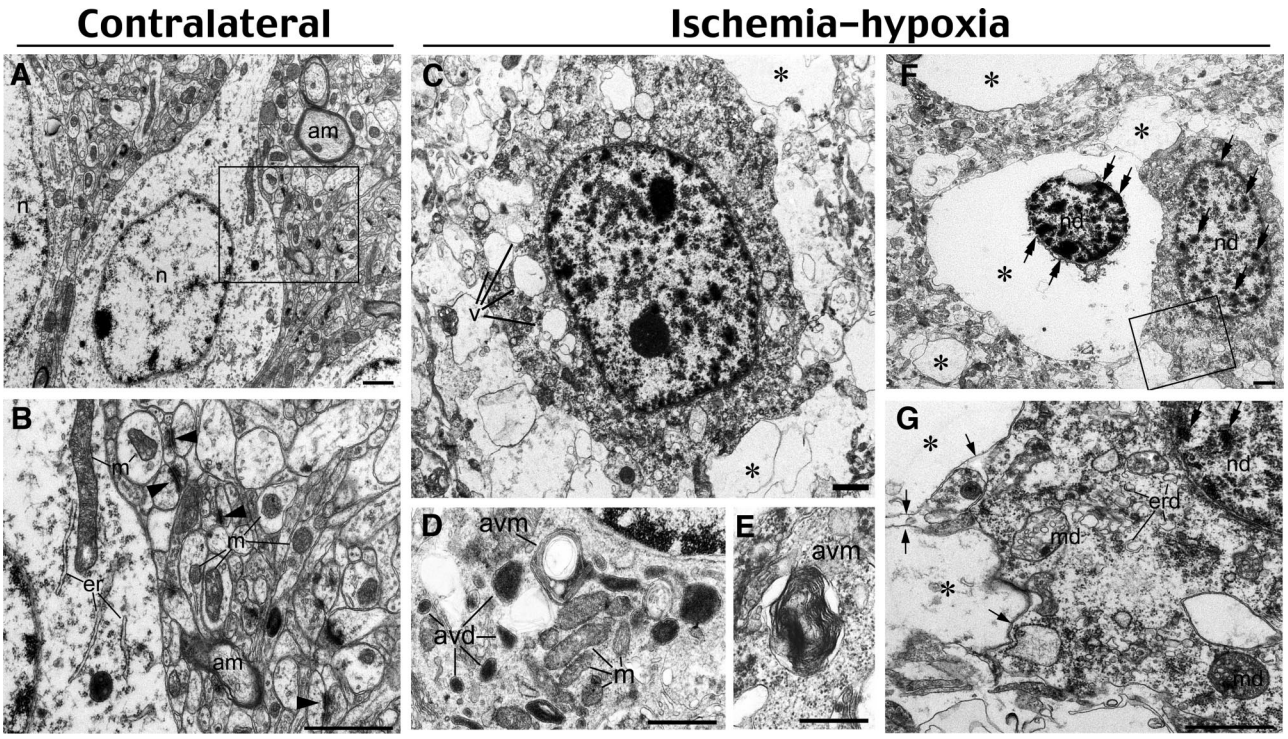

Figure 7. Ischemia-hypoxia induces vacuolization and lysis of cellular organelles. **A** and **B:** Contralateral hemisphere demonstrates normal structures of neuron cell body and neuropil. Notice homogenous nuclear chromatin (n), myelinated axons (am), intact mitochondria (m), *cis*-terns of endoplasmic reticulum (er), and numerous synapses (**arrowheads**). **C–G:** Damaged neurons in the cerebral cortex at 6 hours after ischemia-hypoxia show multiple vacuoles (v in **C**) in the cytoplasm and different degrees of cell destruction. Electron micrographs of the cytoplasm in less damaged neurons (**D** and **E**; notice intact mitochondria, m) exhibit autophagy-like vacuoles containing electron-dense material (avd) and whorls of membranous material (avm). In more advanced cell destruction, many cells demonstrate near-complete lysis of organelles (**asterisks** in **C**, **F**, and **G**), but the plasma membrane of such cells are preserved (**arrows** in **G**). Moderately damaged cells (**G**) display fragmented endoplasmic reticulum membranes (erd), condensed chromatin (**double arrows**) in damaged nuclei (nd), and swollen mitochondria (md) containing electron transparent matrix. Condensation of chromatin (**double arrows** in **F** and **G**) in damaged nuclei might be a result of proapoptotic reaction or represent aborted apoptosis. **B** and **G** represent enlarged framed areas in **A** and **F**, respectively. Scale bars: 1 μm (**A–C**, **F**, **G**); 0.5 μm (**D**, **E**).

the activated form of caspase-3 on immunoblots (data not shown). Because caspase-3 is a final common mediator of apoptosis,[38–39] the lack of biochemical evidence of caspase-3 activation suggests that apoptosis is not a major route of cell death in this model. Indeed, only a small number of cells were detected by the TUNEL stain (indicating double-strand DNA breaks in apoptosis) in the hippocampal CA1 region at both 6 and 24 hours after ischemia-hypoxia (Figure 6, E and H). The frequency of TUNEL-positive cells was even lower in the cortex, striatum, thalamus, and other regions of the hippocampus. In addition, few CA1 hippocampal neurons showed strong labeling by the DNA PANT stain indicating single-strand DNA damage (Figure 6, F and I). These results suggest that although cerebral ischemia-hypoxia initiates the early events of apoptosis, the majority of damaged neurons do not complete the full process of apoptosis. This pattern of aborted apoptosis is similar to that described in the MCAO model.[41]

Ischemia-Hypoxia Induces Autophagic/Lysosomal Cell Death

To further investigate the mode of cell death after cerebral ischemia-hypoxia, we used electron microscopy to examine the morphology of the damaged neurons at 6 (Figure 7) and 18 hours (data not shown). Neurons on the contralateral side of the brain appeared to be healthy with normal endoplasmic reticulum, mitochondria, myelinated axons, and synapses (Figure 7, A and B). In contrast, cortical neurons on the challenged side showed vacuole-associated damage ranging from cells harboring multiple cytoplasmic vacuoles (Figure 7C) to cells completely lacking cytoplasmic contents (Figure 7F). There was also diffuse myelin degeneration and loss of synapses (Figure 7, compare B and G). In less damaged neurons, judging from the morphology of healthy mitochondria, there were many vacuole-related structures containing electron-dense material (Figure 7D, avd) or whorls of membranous material (Figure 7, D and E; avm). These structures resemble autophagic vacuoles previously described in delayed neuronal death after global ischemia[10] or in sympathetic neurons after the withdrawal of nerve growth factors.[42] More severely damaged neurons showed condensed chromatin in the nucleus, cup-shaped endoplasmic reticulum fragments, swollen mitochondria, and vacuoles that contain little material (Figure 7G, asterisk) in the cytoplasm. Moreover, many severely damaged neurons exhibited a shrunken nucleus with condensed chromatin surrounded by extensively lysed cytoplasm but retained an intact plasma membrane (Figure 7F). These morphological features are not typical apoptosis or

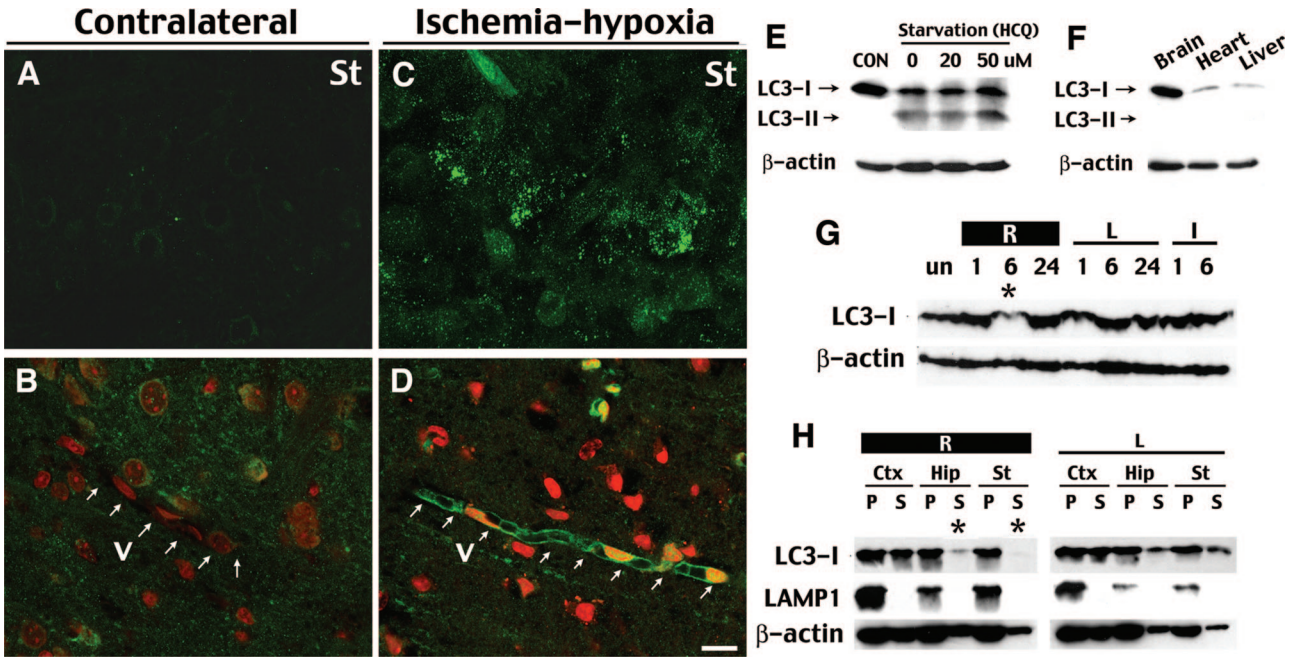

Figure 8. Cerebral ischemia-hypoxia causes redistribution of LC3 proteins indicating autophagy. **A** and **C:** At 6 to 18 hours after ischemia-hypoxia, some cells on the lesion side in the striatum (St) in transgenic GFP-LC3 mice display numerous bright, punctate fluorescent dots (**C**), whereas those on the contralateral side (**A**) and in the unchallenged brains (not shown) exhibit a dim and diffuse pattern of green fluorescence. **B** and **D:** At 18 hours after ischemia-hypoxia, many brain vessels (V) on the lesion side (**D**) express a higher level of GFP-LC3 fluorescence with punctate dots in the endothelial cells, whereas the blood vessels in the contralateral tissue (**B**) lack the fluorescence. **A** and **C** and **B** and **D** were photographed with a confocal microscope using the same laser strength. Nuclei in **B** and **D** are counterstained by ethidium homodimer-1 (red fluorescence). **E:** Immunoblot against LC3 in HEK293 cells in regular medium (10% fetal bovine serum in Dulbecco's modified Eagle's medium) or starvation medium [Hanks' balanced salt solution with hydrochloroquine (HCQ) to inhibit the lysosomes] for 4 hours. Starvation caused a LC3-II band conversion as well as reduction of the LC3-I protein. **F:** Immunoblot showed that the brain in newborns has a higher lever of the LC3-I band compared to the heart and liver. **G:** Immunoblots of the extracts from lateral hemisphere showed a reduction of LC3 protein on the lesion side (R) at 6 hours after ischemia-hypoxia. **H:** Brain tissues were fractionated into supernatant (S) and pellet (P) after centrifugation at 100,000 × *g*, and subjected to LC3, LAMP-1 (a lysosome marker), and β-actin immunoblotting. This analysis shows a selective reduction of LC3 protein in the soluble fraction at 6 hours in the hippocampus (Hip) and the striatum (St) on the ischemia-hypoxia side, but not on the contralateral side. Immunoblot is representative of three independent experiments and images shown are representative for four mice at each time point. Scale bar = 10 μm.

necrosis. Instead, they suggest induction of the autophagosomal-lysosomal compartment of programmed cell death.[43–45]

Macroautophagy (generally referred to as autophagy) is a main route for sequestration of the cytoplasm into the lysosome.[7] The electron microscopy morphology of the damaged neurons prompted us to examine whether autophagy is involved in cell death after cerebral ischemia-hypoxia. To do so, we examined the protein level and subcellular distribution of LC3[46] and GFP immunofluorescence in the GFP-LC3 transgenic mice.[18] LC3, the microtubule-associated protein 1A light chain 3, is normally located throughout the cytoplasm[47] but becomes concentrated in autophagosomes during autophagy.[46,48] Thus, transgenic mice expressing GFP-LC3 will show bright, punctate GFP immunofluorescence in the cytoplasm when the cells are undergoing autophagy.[18] Indeed, in GFP-LC3 mice challenged by cerebral ischemia-hypoxia, clusters of neurons on the ipsilateral side displayed numerous bright, punctate green fluorescent dots compared to neurons on the contralateral side at both 6 and 18 hours after ischemia-hypoxia (Figure 8, A and C). In addition, many blood vessels in the peri-infarct regions showed a higher level of GFP-LC3 expression and punctate GFP-LC3 dots in the endothelial cells at 18 hours (Figure 8, B and D).

When associated with autophagosomes, LC3 typically exhibits a different apparent mobility in electrophoresis, changing from 18 kd to 16 kd, and is commonly referred to as LC3-II band.[46] After autophagosomes are fused with lysosomes, LC3 is either released from autophagolysosomes or becomes degraded within.[48] Pilot experiments established that the reduction of LC3-I and conversion to the LC3-II band could be detected by immunoblots in HEK293 cells after starvation (Figure 8E). The pilot experiments also showed a higher level of LC3-I protein expression in the brain than in the heart and liver in newborns, which may relate to the role of LC3 as a microtubule-associated protein (Figure 8F).[47] Surprisingly, our Western blot analysis did not detect the LC3-II band conversion after ischemia-hypoxia, but did detect a transient reduction of LC3-I protein on the lesion side at 6 hours (Figure 8G). Immunoblot after cell fractionation further revealed that LC3 was primarily reduced in the supernatant (S), but not the pellet (P) fraction after centrifugation at 100,000 × *g*, in the hippocampus and striatum (Figure 8F). Together, the induction of GFP-LC3 immunofluorescence supports the involvement of autophagy, and the transient reduction of LC3-I may be caused by a rapid turnover of LC3 proteins by autophagolysosome processing after cerebral ischemia-hypoxia. Nonetheless, we cannot exclude the possibility

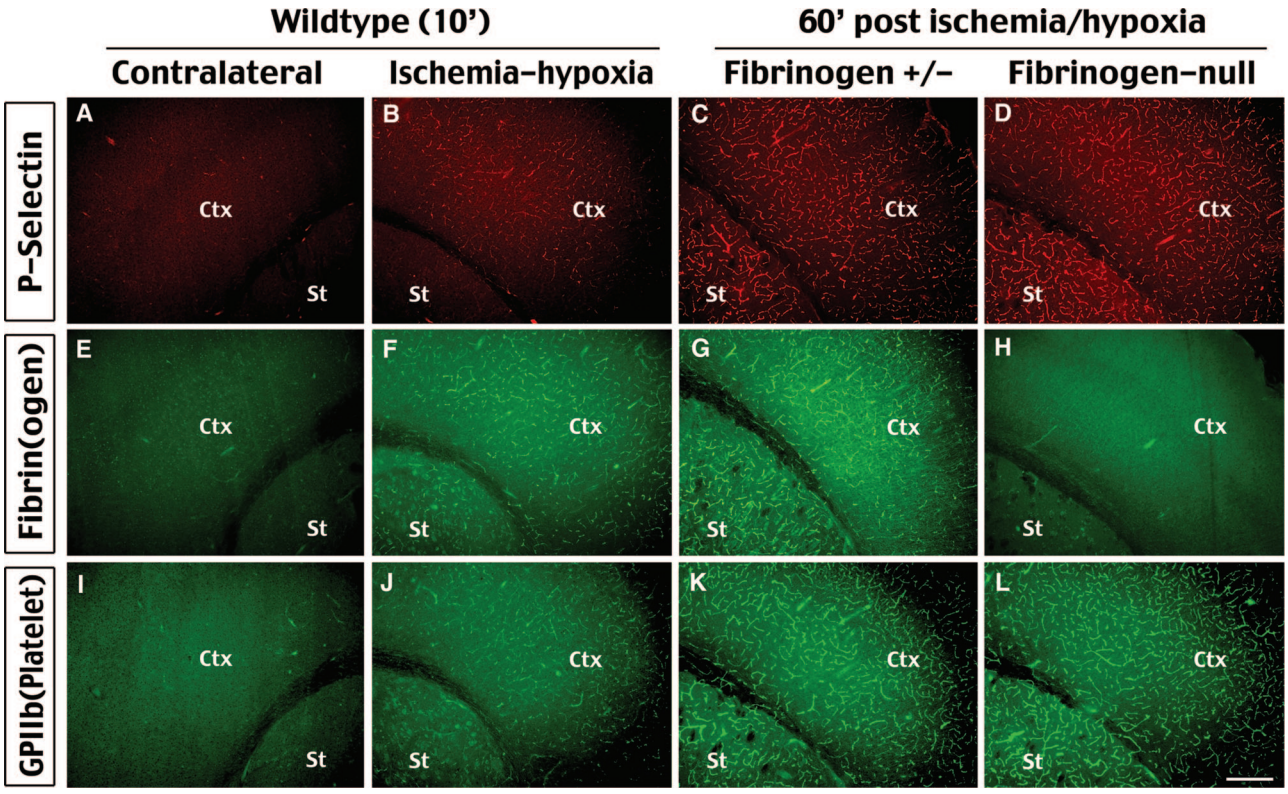

Figure 9. Cerebral ischemia-hypoxia rapidly activates endothelial cells and induces coagulation. Immunostaining of P-selectin (**A–D**), fibrinogen (**E–H**), and GPIIb (**I–L**, a platelet surface marker) are performed at indicated times after ischemia-hypoxia. This analysis shows induction of P-selectin expression and fibrin(ogen) and platelet accumulation in the blood vessels in the striatum (St) and cortex (Ctx) on the lesion side (**B**, **F**, **J**), but not on the contralateral side (**A**, **E**, **I**), at 10 minutes after ischemia-hypoxia in wild-type mice. Notice the area of coagulation matches the area of reperfusion deficits in Figure 4C. Mice heterozygous for *fibrinogen*-null mutation show broad P-selectin expression (**C**), fibri(ogen) deposition (**G**), and platelet accumulation (**K**) at 1 hour after ischemia-hypoxia similar to the pattern in the wild-type mice (data not shown). *Fibrinogen*-null mice lacked fibrinogen deposition (**H**) while retaining P-selectin expression (**D**) and platelet accumulation (**L**) as their heterozygous littermates. Shown pictures are representative of three animals for each immunostaining. Scale bar = 200 μm.

that our procedure for protein extraction from tissues may have masked the difference of apparent mobility between LC3-I and LC3-II in electrophoresis.

Cerebral Ischemia-Hypoxia Induces Acute Fibrin Deposition Leading to Reperfusion Deficits

Our analyses suggested that cerebral ischemia-hypoxia induces acute and persistent reperfusion deficits (Figures 3B and 4B), which may be a cause of large hemispheric infarction. One potential mechanism of the severe reperfusion deficits is hypoxia-induced procoagulation properties of endothelial cells and resultant thrombus formation.[3,4] To test this hypothesis, we examined the expression of P-selectin (a marker of endothelial cell activation[49,50]), integrin α 2b (a platelet surface marker, also known as glycoprotein IIb, GPIIb),[49] and fibrin in the blood vessels after ischemia-hypoxia. We found that at as early as 10 minutes after the hypoxia interval, there was substantial P-selectin, fibrin, and GPIIb (ie, platelet integrin subunit α_M) staining in the striatum and the anterior cerebral cortex on the carotid artery-occluded side of the brain (Figure 9, B, F, and J). These proteins were also detected at 1 hour after the hypoxia interval in both heterozygous for the *fibrinogen* Aα-null allele (*Fib*$^{+/-}$ mice) (Figure 9, C, G, and K)[19] and wild-type mice (data not shown). In contrast, the immunostaining for these parameters was negative on the contralateral side of brain after ischemia-hypoxia (Figure 9, A, E, and I) or after unilateral carotid occlusion (data not shown). Importantly, although focal ischemia can trigger fibrin deposition and platelet accumulation in the blood vessels, these events typically occur in a delayed manner after transient hyperemia.[50–53]

The rapid onset of fibrin deposition after ischemia-hypoxia suggests an important role in causing reperfusion deficits and brain infarction. To test this hypothesis, we examined the responses of *fibrinogen*-null mice[19] and their heterozygous littermates to cerebral ischemia-hypoxia. Like their *fibrinogen*-expressing littermates, *fibrinogen*-null mice exhibited P-selectin and GPIIb deposition immediately (data not shown) or at 1 hour after ischemia-hypoxia (Figure 9, D and L). This is consistent with the known capacity of *Fib*$^{-/-}$ mice to support unstable platelet deposition after vascular injury. However, as expected, challenged fibrinogen-deficient mice exhibited no detectable fibrin deposition (Figure 9H). This result suggests that *fibrinogen*-null mice are also susceptible to cerebral ischemia-hypoxia induced endothelial cell activation and platelet accumulation. However, *fibrinogen*-null mice showed a significantly improved recovery of brain perfusion after reversible RCCA occlusion and 40-minute hypoxia (Figure 10, A and B). On RCCA occlu-

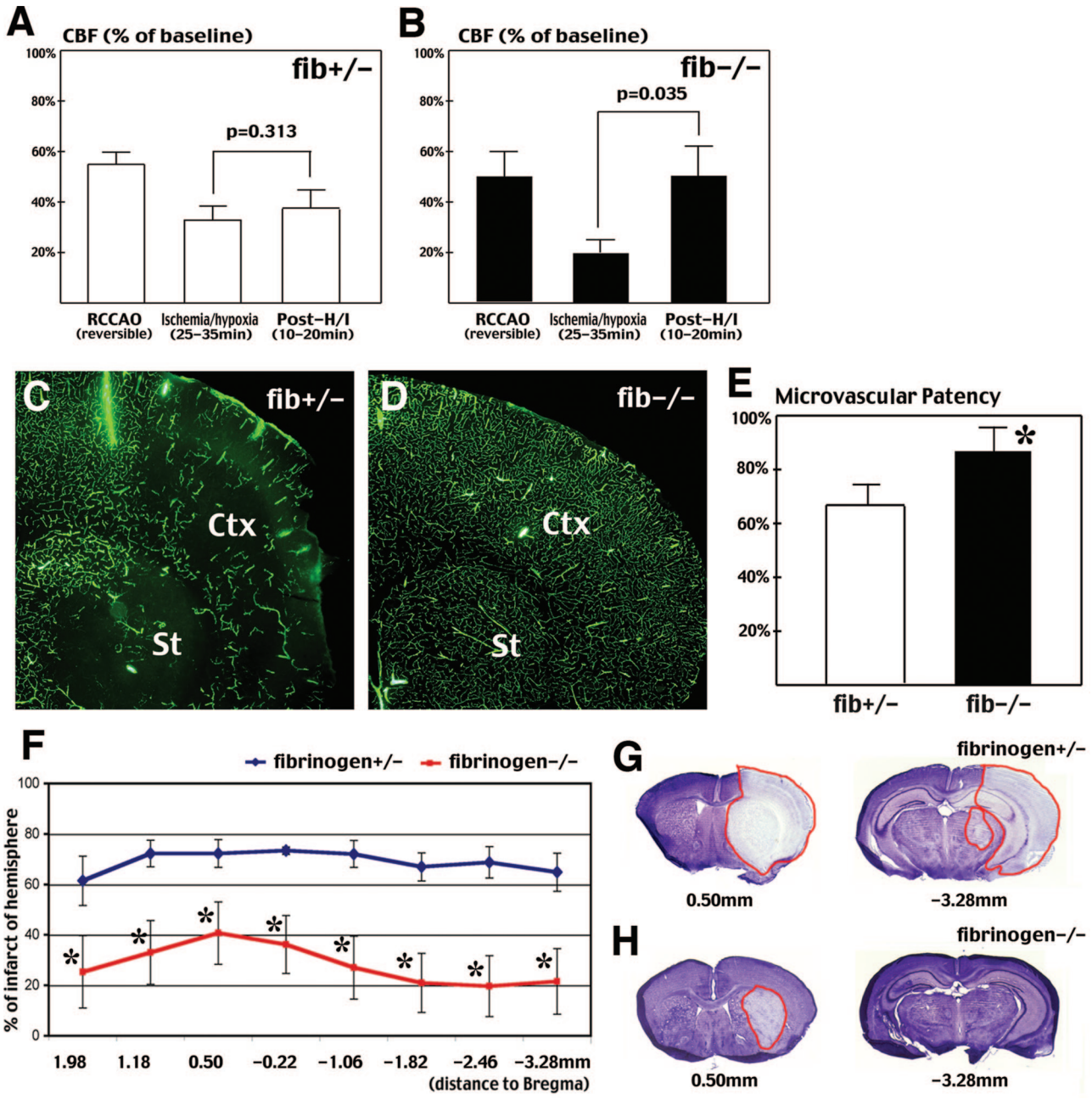

Figure 10. Fibrin deposition is a major component of reperfusion impediment and subsequent infarction after cerebral ischemia-hypoxia. **A** and **B:** Laser Doppler flowmetry indicates that CBF significantly rebounds in fibrinogen-deficient mice (**B**) after ischemia-hypoxia, but not in their heterozygous littermates (**A**) (n = 3 for each genotype). Mice that died during hypoxia were excluded from this analysis. **C** and **D:** FITC-dextran infusion shows greater perfusion deficits in heterozygous *fibrinogen*-null (**C**) than homozygous *fibrinogen*-null (**D**) mice at 1 hour after ischemia-hypoxia. **E:** Quantification of the FITC-dextran fluorescence shows significantly greater microvascular patency at four different brain sections in the *fibrinogen*-null mice (n = 6 for each genotype; $^*P < 0.05$). **F–H:** At 24 hours after right common carotid occlusion and 35-minute hypoxia, Nissl stain indicates significant reduction of brain infarction ($^*P < 0.05$) in homozygous *fibrinogen*-null mice (red line, n = 6) than in heterozygous littermates (blue line, n = 4, excluding two cases of mortality). **G** and **H:** Nissl stain of representative sections shows a typical infarction pattern in fibrinogen heterozygous (**G**) mice and a limited infarction in homozygous *fibrinogen*-null mice (**H**).

sion, the CBF on the ipsilateral side of the cerebral cortex dropped to 54.8% and 49.7% of the preocclusion value in the control and *fibrinogen*-null mice, respectively. Between 25 to 35 minutes of hypoxia, the control mice retained an average of 32.6% of the CBF that increased to 37.8% at 10 to 20 minutes after ischemia-hypoxia (Figure 10A, n = 3), or showed a 17% residual CBF but died either during or immediately after the hypoxia interval (n = 4). In contrast, in *fibrinogen*-null mice, the CBF declined to 19.8% between 25 to 35 minutes of hypoxia but rebounded to 50.2% at 10 to 20 minutes after the release of RCCA occlusion and hypoxia (n = 3). Furthermore, at 1 hour after permanent RCCA occlusion and 40-minute hypoxia, 87.7% of the expected blood vessel area was filled with intracardial injected FITC-dextran in the fibrinogen-null mouse brains (Figure 10, D and E; n = 6), whereas only 67.9% of the expected blood vessel area was filled with the fluorescent dye in the control mice

(Figure 10, C and E; $n = 6$; $P < 0.05$). In addition, *fibrinogen*-null mice showed better outcomes after cerebral ischemia-hypoxia. At 24 hours after RCCA occlusion and 35-minute hypoxia, two of six control mice had died whereas none of six *fibrinogen*-null mice died. Nissl stain and quantitative analysis in surviving animals showed that *fibrinogen*-null mice have significantly less infarction throughout the brain (Figure 10, F–H). Together, these results indicate that fibrinogen-deficiency improves cerebral reperfusion and reduces brain infarction after ischemia-hypoxia.

Discussion

Ischemic stroke involves a complex array of pathological processes and induces highly variable outcomes that are modified by many factors beyond reduction of the CBF. Imaging studies have shown that predictors of irreversible tissue damage are reduction of the oxygen extraction fraction and the cerebral metabolic rate of oxygen.[2] These results suggest that hypoxia is important for determining whether the brain tissue receiving inadequate blood supply will survive or die. In this context, the Levine/Vannucci model is unique in that it combines ischemia and hypoxia.[13,14]

Although the Levine/Vannucci procedure (unilateral carotid occlusion plus hypoxia) was originally developed in adult rats in the 1960s, it became popular in the 1980s as an experimental model of perinatal hypoxic-ischemic brain damage.[13,14] A criticism of the Levine/Vannucci model has been that it produces too inconsistent brain damage in adult animals. However, recent studies indicate that controlling the body temperature and/or adjusting the duration of hypoxia improves the consistency of brain damage in adult rodents.[11,15] We used an alternative approach in this study by directly infusing the hypoxic gas to individual animals after carotid artery occlusion while controlling the core temperature throughout the hypoxia interval. This allows for rapid adjustment of the body temperature, and permits continuous monitoring of the CBF during ischemia-hypoxia. We found that the combination of unilateral carotid occlusion and hypoxia diminishes the CBF to levels seen with focal ischemia models (Figure 3). Subsequently, it causes protracted reperfusion deficits (Figure 4), large brain infarction, and brain edema (Figure 2). Moreover, this modified model produces consistent brain infarction (Figure 1).

An additional merit of this modified Levine/Vannucci model of stroke is that it does not require sophisticated surgical expertise. Hence, it can be easily established in any laboratory to facilitate comparisons of results between different research laboratories. Nonetheless, there are several technical concerns of this new model. First, our preliminary experiments showed that the 129sv strain has smaller infarctions than C57BL/6 and BALB/c strains (unpublished data), similar to the situation with focal ischemia models.[54,55] Thus, the exact experimental parameters for the modified Levine/Vannucci model need to be determined for each mouse strain or mutants with a mixed genetic background. Second, in the traditional Levine/Vannucci model, animals are exposed to the hypoxia after they have recovered from the anesthesia, whereas our modified model relies on the use of anesthesia to restrain the animal during the hypoxia interval. Thus, the choice and effects of anesthesia to be used in this new model must be considered.

Ischemia-Hypoxia Precipitates Thrombosis Leading to Cerebral Reperfusion Deficits

One of the most surprising findings of the present study is that the decline of CBF in conjunction with hypoxia is sufficient to induce rapid microvascular thrombosis and fibrin deposition within the brain (Figure 9). By analyzing challenged *fibrinogen*-null mice we have established that fibrin(ogen) plays an important role the reperfusion deficits and brain infarction (Figure 10). These results suggest that if cerebral ischemia is accompanied with hypoxia, this combination can precipitate local coagulation and impede reperfusion after ischemia, similar to the previously described no-reflow phenomenon after cerebral ischemia[5] and cardiac arrest.[56] It seems likely that fibrin stabilization of platelet thrombi is a major determinant of brain tissue damage. If so, we would predict that a similar, if not more impressive, protection from tissue damage could be realized in mice with a profound defect in platelet function. It is also conceivable that fibrin-mediated inflammatory processes drive secondary tissue damage in the brain. Thus, the modified Levine/Vannucci model described here may be useful for testing new therapies to restore postischemic reperfusion in the face of thrombolytic agents and other approaches to reopened large vessels.

Regarding the mechanism of ischemia/hypoxia-induced thrombosis, it seems likely that hypoxia alters the balance between anti- and procoagulation properties of the endothelial cells in cerebral blood vessels. Although focal ischemia can trigger platelet accumulation and fibrin deposition, these events typically show a late-onset after a transient hyperemia phase.[49,53] In contrast, the present study shows that the combination of ischemia and hypoxia precipitates these events almost immediately. Understanding the mechanism by which combined ischemia-hypoxia alters the homeostatic properties of endothelial cells in cerebral vessels may suggest novel prophylactic therapies in clinical situations when the imminent risk of cerebral ischemia and hypoxia is high, such as coronary bypass surgery.

Concurrent Induction of Autophagy, Apoptosis, and Necrosis in Ischemic Stroke

Our analysis demonstrates early IL-1β production after cerebral ischemia-hypoxia, similar to the condition in focal ischemia (Figure 5).[31,32] We also show parallel induction of anti-apoptotic (ERK/AKT/Hsp70) and proapoptotic (AIF/caspase) signaling pathways in the threatened, yet viable tissues before they infarct (Figure 6). Although the

combined cerebral ischemia-hypoxia induces the upstream caspases including caspase-8 and -9, it only leads to very limited caspase-3 activation and apoptosis (Figures 6 and 7). These results suggest that the process of apoptosis is interrupted by other cellular events using this particular model of stroke and support other studies questioning the significance of apoptosis in focal cerebral ischemia.[57–59]

Electron microscopy showed vacuolization and extensive lysis of cytoplasmic contents in the damaged cells, suggesting an induction of the autophagic-lysosomal compartment of programmed cell death.[43–45] This is supported by the condensation of GFP-LC3 fluorescence and the disappearance of LC3 proteins in the cytosol fraction after cerebral ischemia-hypoxia (Figure 8). Although we did not detect the LC3-II band in immunoblots, this could be because the autophagosomes rapidly fuse with lysosomes in the brain after ischemia-hypoxia thus preventing LC3-II accumulation.[48] However, we find that the cytosol fraction of LC3 is rapidly depleted in the brain, presumably inside autophagolysosomes. The remaining pellet-fraction of LC3 in the brain may reflect microtubule-associated protein that is not related to autophagy because it does not appear to be the 16-kd LC3-II band.[47] It should also be noted that our results do not exclude the possibility of additional mechanisms besides LC3-related autophagy to activate lysosomes and digest the cytoplasm of damaged cells.

Because morphological features of necrosis were also detected by electron microscopy, these results indicate that cerebral ischemia-hypoxia initiates all three pathways of cell death including necrosis, apoptosis, and autophagy. It is possible that one or more of these mechanisms may be occurring in a given cell particularly throughout time. Thus, the damaged cells can display morphological features of multiple forms of cell-death and the brain tissue as a whole exhibits biochemical hallmarks of all these pathways. Although autophagy appears to be occurring after cerebral ischemia-hypoxia, its biological relevance is uncertain. It could be an important mechanism of cell self-destruction. Alternatively, autophagy may protect neurons by degrading damaged organelles to abrogate apoptosis or generating energy to delay the onset of ionic imbalance and necrosis after cerebral ischemia-hypoxia. Future studies that either enhance or inhibit autophagy are needed to determine its biological functions in stroke.

Acknowledgments

We thank K.A. Hossmann, G.J. del Zoppo, and P.G. Clarke for helpful discussion; R.G. Pratt, W.-L. Weng, A. Sprodes, G.L. Keller, and the Cincinnati Children's Hospital Medical Center Veterinary Service staff for excellent technical support; and the Riken BioResource Center (Tsukuba, Japan) for providing the GFP-LC3 mice.

References

1. Baron JC: Perfusion thresholds in human cerebral ischemia: historical perspective and therapeutic implications. Cerebrovasc Dis 2001, 11(Suppl 1):S2–S8
2. Sobesky J, Zaro Weber O, Lehnhardt FG, Hesselmann V, Neveling M, Jacobs A, Heiss WD: Does the mismatch match the penumbra? Magnetic resonance imaging and positron emission tomography in early ischemic stroke. Stroke 2005, 36:980–985
3. Yan SF, Mackman N, Kisiel W, Stern DM, Pinsky DJ: Hypoxia/hypoxemia-induced activation of the procoagulant pathways and the pathogenesis of ischemia-associated thrombosis. Arterioscler Thromb Vasc Biol 1999, 19:2029–2035
4. Ten VS, Pinsky DJ: Endothelial response to hypoxia: physiologic adaptation and pathologic dysfunction. Curr Opin Crit Care 2002, 8:242–250
5. Majno G, Ames AI, Chiang J, Wright R: No reflow after cerebral ischaemia. Lancet 1967, 2:569–570
6. Rezkalla SH, Kloner RA: No-reflow phenomenon. Circulation 2002, 105:656–662
7. Levine B, Klionsky DJ: Development by self-digestion: molecular mechanisms and biological functions of autophagy. Dev Cell 2004, 6:463–477
8. Clarke PG: Developmental cell death: morphological diversity and multiple mechanisms. Anat Embryol (Berl) 1990, 181:195–213
9. Yan L, Vatner DE, Kim SJ, Ge H, Masurekar M, Massover WH, Yang G, Matsui Y, Sadoshima J, Vatner SF: Autophagy in chronically ischemic myocardium. Proc Natl Acad Sci USA 2005, 102:13807–13812
10. Nitatori T, Sato N, Waguri S, Karasawa Y, Araki H, Shibanai K, Kominami E, Uchiyama Y: Delayed neuronal death in the CA1 pyramidal cell layer of the gerbil hippocampus following transient ischemia is apoptosis. J Neurosci 1995, 15:1001–1011
11. Zhu C, Wang X, Xu F, Bahr BA, Shibata M, Uchiyama Y, Hagberg H, Blomgren K: The influence of age on apoptotic and other mechanisms of cell death after cerebral hypoxia-ischemia. Cell Death Differ 2005, 12:162–176
12. Degterev A, Huang Z, Boyce M, Li Y, Jagtap P, Mizushima N, Cuny GD, Mitchison TJ, Moskowitz MA, Yuan J: Chemical inhibitor of nonapoptotic cell death with therapeutic potential for ischemic brain injury. Nat Chem Biol 2005, 1:112–119
13. Levine S: Anoxic-ischemic encephalopathy in rats. Am J Pathol 1960, 36:1–17
14. Rice III JE, Vannucci RC, Brierley JB: The influence of immaturity on hypoxic-ischemic brain damage in the rat. Ann Neurol 1981, 9:131–141
15. Vannucci SJ, Willing LB, Goto S, Alkayed NJ, Brucklacher RM, Wood TL, Towfighi J, Hurn PD, Simpson IA: Experimental stroke in the female diabetic, db/db, mouse. J Cereb Blood Flow Metab 2001, 21:52–60
16. Basu A, Lazovic J, Krady JK, Mauger DT, Rothstein RP, Smith MB, Levison SW: Interleukin-1 and the interleukin-1 type 1 receptor are essential for the progressive neurodegeneration that ensues subsequent to a mild hypoxic/ischemic injury. J Cereb Blood Flow Metab 2005, 25:17–29
17. Busto R, Dietrich WD, Globus MY, Valdes I, Scheinberg P, Ginsberg MD: Small differences in intraischemic brain temperature critically determine the extent of ischemic neuronal injury. J Cereb Blood Flow Metab 1987, 7:729–738
18. Mizushima N, Yamamoto A, Matsui M, Yoshimori T, Ohsumi Y: In vivo analysis of autophagy in response to nutrient starvation using transgenic mice expressing a fluorescent autophagosome marker. Mol Biol Cell 2004, 15:1101–1111
19. Suh TT, Holmback K, Jensen NJ, Daugherty CC, Small K, Simon DI, Potter S, Degen JL: Resolution of spontaneous bleeding events but failure of pregnancy in fibrinogen-deficient mice. Genes Dev 1995, 9:2020–2033
20. Longa EZ, Weinstein PR, Carlson S, Cummins R: Reversible middle cerebral artery occlusion without craniectomy in rats. Stroke 1989, 20:84–91
21. Franklin KBJ, Paxinos G: The Mouse Brain in Stereotaxic Coordinates. San Diego, Academic Press, 1997
22. Kuan CY, Schloemer AJ, Lu A, Burns KA, Weng WL, Williams MT, Strauss KI, Vorhees CV, Flavell RA, Davis RJ, Sharp FR, Rakic P: Hypoxia-ischemia induces DNA synthesis without cell proliferation in

dying neurons in adult rodent brain. J Neurosci 2004, 24:10763–10772
23. Chen J, Jin K, Chen M, Pei W, Kawaguchi K, Greenberg DA, Simon RP: Early detection of DNA strand breaks in the brain after transient focal ischemia: implications for the role of DNA damage in apoptosis and neuronal cell death. J Neurochem 1997, 69:232–245
24. Ding G, Jiang Q, Zhang L, Zhang ZG, Li L, Knight RA, Ewing JR, Wang Y, Chopp M: Analysis of combined treatment of embolic stroke in rat with r-tPA and a GPIIb/IIIa inhibitor. J Cereb Blood Flow Metab 2005, 25:87–97
25. Fishman RA: Brain edema. N Engl J Med 1975, 293:706–711
26. Ginsberg MD: Adventures in the pathophysiology of brain ischemia: penumbra, gene expression, neuroprotection: the 2002 Thomas Willis Lecture. Stroke 2003, 34:214–223
27. Heistad DD, Kontos HA: Cerebral Circulation. Edited by Shepherd JT, Abboud FM, Geiger SR. Bethesda, American Physiological Society, 1983, pp 137–182
28. Williams DS, Detre JA, Leigh JS, Koretsky AP: Magnetic resonance imaging of perfusion using spin inversion of arterial water. Proc Natl Acad Sci USA 1992, 89:212–216
29. Moseley ME, Cohen Y, Mintorovitch J, Chileuitt L, Shimizu H, Kucharczyk J, Wendland MF, Weinstein PR: Early detection of regional cerebral ischemia in cats: comparison of diffusion- and T2-weighted MRI and spectroscopy. Magn Reson Med 1990, 14:330–346
30. Steiner T, Ringleb P, Hacke W: Treatment options for large hemispheric stroke. Neurology 2001, 57(Suppl 2):S61–S8
31. Wang X, Barone FC, Aiyar NV, Feuerstein GZ: Interleukin-1 receptor and receptor antagonist gene expression after focal stroke in rats. Stroke 1997, 28:152–161
32. Allan SM, Rothwell NJ: Cytokines and acute neurodegeneration. Nat Rev Neurosci 2001, 2:734–744
33. Noshita N, Lewen A, Sugawara T, Chan PH: Evidence of phosphorylation of Akt and neuronal survival after transient focal cerebral ischemia in mice. J Cereb Blood Flow Metab 2001, 21:1442–1450
34. Ferrer I, Friguls B, Dalfo E, Planas AM: Early modifications in the expression of mitogen-activated protein kinase (MAPK/ERK), stress-activated kinases SAPK/JNK and p38, and their phosphorylated substrates following focal cerebral ischemia. Acta Neuropathol (Berl) 2003, 105:425–437
35. Kokubo Y, Liu J, Rajdev S, Kayama T, Sharp FR, Weinstein PR: Differential cerebral protein synthesis and heat shock protein 70 expression in the core and penumbra of rat brain after transient focal ischemia. Neurosurgery 2003, 53:186–190
36. Sharp FR, Lu A, Tang Y, Millhorn DE: Multiple molecular penumbras after focal cerebral ischemia. J Cereb Blood Flow Metab 2000, 20:1011–1032
37. Ferrer I, Planas AM: Signaling of cell death and cell survival following focal cerebral ischemia: life and death struggle in the penumbra. J Neuropathol Exp Neurol 2003, 62:329–339
38. Nicholson DW, Ali A, Thornberry NA, Vaillancourt JP, Ding CK, Gallant M, Gareau Y, Griffin PR, Labelle M, Lazebnik YA, Munday NA, Raju SM, Smulson ME, Yamin TT, Yu VL, Miller DK: Identification and inhibition of the ICE/CED-3 protease necessary for mammalian apoptosis. Nature 1995, 376:37–43
39. Kuida K, Zheng TS, Na S, Kuan C, Yang D, Karasuyama H, Rakic P, Flavell RA: Decreased apoptosis in the brain and premature lethality in CPP32-deficient mice. Nature 1996, 384:368–372
40. Hillhouse EW, Kida S, Iannotti F: Middle cerebral artery occlusion in the rat causes a biphasic production of immunoreactive interleukin-1beta in the cerebral cortex. Neurosci Lett 1998, 249:177–179
41. Benchoua A, Guegan C, Couriaud C, Hosseini H, Sampaio N, Morin D, Onteniente B: Specific caspase pathways are activated in the two stages of cerebral infarction. J Neurosci 2001, 21:7127–7134
42. Xue L, Fletcher GC, Tolkovsky AM: Autophagy is activated by apoptotic signalling in sympathetic neurons: an alternative mechanism of death execution. Mol Cell Neurosci 1999, 14:180–198
43. Edinger AL, Thompson CB: Death by design: apoptosis, necrosis and autophagy. Curr Opin Cell Biol 2004, 16:663–669
44. Kroemer G, Jaattela M: Lysosomes and autophagy in cell death control. Nat Rev Cancer 2005, 5:886–897
45. Tsujimoto Y, Shimizu S: Another way to die: autophagic programmed cell death. Cell Death Differ 2005,12(Suppl 2):S1528–S1534
46. Kabeya Y, Mizushima N, Ueno T, Yamamoto A, Kirisako T, Noda T, Kominami E, Ohsumi Y, Yoshimori T: LC3, a mammalian homologue of yeast Apg8p, is localized in autophagosome membranes after processing. EMBO J 2000, 19:5720–5728
47. Mann SS, Hammarback JA: Molecular characterization of light chain 3. A microtubule binding subunit of MAP1A and MAP1B. J Biol Chem 1994, 269:11492–11497
48. Mizushima N: Methods for monitoring autophagy. Int J Biochem Cell Biol 2004, 36:2491–2502
49. del Zoppo GJ, Mabuchi T: Cerebral microvessel responses to focal ischemia. J Cereb Blood Flow Metab 2003, 23:879–894
50. Okada Y, Copeland BR, Mori E, Tung MM, Thomas WS, del Zoppo GJ: P-selectin and intercellular adhesion molecule-1 expression after focal brain ischemia and reperfusion. Stroke 1994, 25:202–211
51. Okada Y, Copeland BR, Fitridge R, Koziol JA, del Zoppo GJ: Fibrin contributes to microvascular obstructions and parenchymal changes during early focal cerebral ischemia and reperfusion. Stroke 1994, 25:1847–1853
52. Zhang R, Chopp M, Zhang Z, Jiang N, Powers C: The expression of P- and E-selectins in three models of middle cerebral artery occlusion. Brain Res 1998, 785:207–214
53. Ishikawa M, Cooper D, Russell J, Salter JW, Zhang JH, Nanda A, Granger DN: Molecular determinants of the prothrombogenic and inflammatory phenotype assumed by the postischemic cerebral microcirculation. Stroke 2003, 34:1777–1782
54. Fujii M, Hara H, Meng W, Vonsattel JP, Huang Z, Moskowitz MA: Strain-related differences in susceptibility to transient forebrain ischemia in SV-129 and C57black/6 mice. Stroke 1997, 28:1805–1811
55. Majid A, He YY, Gidday JM, Kaplan SS, Gonzales ER, Park TS, Fenstermacher JD, Wei L, Choi DW, Hsu CY: Differences in vulnerability to permanent focal cerebral ischemia among 3 common mouse strains. Stroke 2000, 31:2707–2714
56. Fischer M, Hossmann KA: No-reflow after cardiac arrest. Intensive Care Med 1995, 21:132–141
57. Colbourne F, Sutherland GR, Auer RN: Electron microscopic evidence against apoptosis as the mechanism of neuronal death in global ischemia. J Neurosci 1999, 19:4200–4210
58. Northington FJ, Ferriero DM, Graham EM, Traystman RJ, Martin LJ: Early neurodegeneration after hypoxia-ischemia in neonatal rat is necrosis while delayed neuronal death is apoptosis. Neurobiol Dis 2001, 8:207–219
59. Joly LM, Mucignat V, Mariani J, Plotkine M, Charriaut-Marlangue C: Caspase inhibition after neonatal ischemia in the rat brain. J Cereb Blood Flow Metab 2004, 24:124–131